nature communications

Article

https://doi.org/10.1038/s41467-024-50770-7

A broadly cross-reactive i-body to AMA1 potently inhibits blood and liver stages of *Plasmodium* parasites

Received: 12 December 2023

Accepted: 19 July 2024

Published online: 22 August 2024

Check for updates

Dimuthu Angage[1], Jill Chmielewski[2], Janesha C. Maddumage[1], Eva Hesping[3,4], Sabrina Caiazzo[3,4], Keng Heng Lai[2], Lee Ming Yeoh[5,6], Joseph Menassa[1], D. Herbert Opi[5,6,7], Callum Cairns[1], Hamsa Puthalakath[1], James G. Beeson[5,7,8], Marc Kvansakul[1], Justin A. Boddey[3,4], Danny W. Wilson[2,5,9], Robin F. Anders[1] & Michael Foley[1,10]

Apical membrane antigen-1 (AMA1) is a conserved malarial vaccine candidate essential for the formation of tight junctions with the rhoptry neck protein (RON) complex, enabling *Plasmodium* parasites to invade human erythrocytes, hepatocytes, and mosquito salivary glands. Despite its critical role, extensive surface polymorphisms in AMA1 have led to strain-specific protection, limiting the success of AMA1-based interventions beyond initial clinical trials. Here, we identify an i-body, a humanised single-domain antibody-like molecule that recognises a conserved pan-species conformational epitope in AMA1 with low nanomolar affinity and inhibits the binding of the RON2 ligand to AMA1. Structural characterisation indicates that the WD34 i-body epitope spans the centre of the conserved hydrophobic cleft in AMA1, where interacting residues are highly conserved among all *Plasmodium* species. Furthermore, we show that WD34 inhibits merozoite invasion of erythrocytes by multiple *Plasmodium* species and hepatocyte invasion by *P. falciparum* sporozoites. Despite a short half-life in mouse serum, we demonstrate that WD34 transiently suppressed *P. berghei* infections in female BALB/c mice. Our work describes the first pan-species AMA1 biologic with inhibitory activity against multiple life-cycle stages of *Plasmodium*. With improved pharmacokinetic characteristics, WD34 could be a potential immunotherapy against multiple species of *Plasmodium*.

Progress in reducing the global burden of malaria has stalled, and numerous challenges to established interventions have evolved, highlighting the need for new interventions to prevent malaria[1]. *Plasmodium falciparum* accounts for most of the malaria-induced morbidity and mortality worldwide, with *P. vivax* being the second major cause[1–3]. Invasion of erythrocytes by *Plasmodium* merozoites initiates all the clinical manifestations of malaria[4]. The invasion process is fast, sequential, and tightly regulated by multiple interactions between parasite ligands and receptors on the erythrocyte surface[5,6]. Following attachment to the erythrocyte membrane, the merozoite reorientates, allowing the apical end to form a tight junction as an entry point for invading host erythrocytes[7]. Parasite antigens involved in this attachment and invasion process have been explored as potential antimalarial blood-stage vaccines and therapeutic targets[8–10].

AMA1 is a micronemal protein released onto the parasite surface following the attachment of the merozoite to the erythrocyte membrane. AMA1 subsequently binds to a hairpin loop in the ectodomain of the RON2 protein on the erythrocyte surface to form a tight junction[11–13]. There is considerable experimental evidence that the AMA1-RON2 complex is also involved in sporozoite invasion of

A full list of affiliations appears at the end of the paper. e-mail: m.foley@latrobe.edu.au

mosquito salivary glands and mammalian hepatocytes[14–16]. AMA1 is one of the few invasion proteins shared between all *Plasmodium* species causing human malaria, although the sequence varies between species. Previously, *Pf*AMA1 was evaluated as a promising vaccine candidate due to its pivotal role in host cell invasion by multiple life-cycle stages of the parasite and being an immunogenic protein targeted by acquired immunity[6,17,18]. However, polymorphisms in AMA1 tend to induce strain-specific protection, and for this reason, clinical development of AMA1 has been challenging[19–23]. Even though a few cross-reactive monoclonal antibodies (mAbs) have been generated against AMA1, these antibodies lacked significant functional activity[24–28].

i-bodies are human single immunoglobulin domains inspired by the structural features of the shark variable new antigen receptor (V_{NAR}) and were designed to overcome some of the limitations of conventional mAbs[29,30]. The i-body consists of a human scaffold (first Ig domain of the human neural cell adhesion molecule) and two regions of hypervariable amino acids constituting complementarity determining regions (CDR) 1 & 3, where they would exist in the V_{NAR}[29,30]. By randomising sequences of CDR1 (fixed length) and CDR3 (variable length), a library containing 10^{10} unique i-bodies was generated. Due to their smaller size compared to conventional antibodies and easy access to cryptic epitopes, i-bodies have been considered as potential therapeutics against diseases such as osteoporosis, idiopathic pulmonary fibrosis, and renal fibrosis[29,31,32]. In this study, we investigated the use of i-bodies to identify novel epitopes in AMA1, an important malaria vaccine candidate.

Phage display was used to identify a novel i-body, WD34, which binds to AMA1 from multiple *Plasmodium* species with low nanomolar affinity. By determining the crystal structures of WD34-AMA1 complexes, we have defined the binding footprint of WD34 in *Pf* and *Pv*AMA1. Using several *Plasmodium* strains and species, we demonstrated the inhibitory role of WD34 in merozoite and sporozoite invasion. Furthermore, we showed that WD34 could transiently suppress *P. berghei* infections in BALB/c mice. Our findings identify WD34 as the first pan-species anti-malarial antibody-like molecule with high invasion inhibitory activity.

Results

Identification of strain transcending i-bodies to AMA1

The i-body library, described by Griffiths et al.[29], was biopanned on recombinant AMA1 (recAMA1) of two *P. falciparum* strains, 3D7 and W2mef (termed haplotype-distance biopanning). These two isoforms of *Pf*AMA1 were chosen because they differ at many of the polymorphic sites in the antigen and show substantial antigenic differences[33–35]. In addition to panning on individual *Pf*AMA1 isoforms, a cross-panning strategy was employed in which phage selected after three rounds of panning on one *Pf*AMA1 isoform were subjected to three further panning rounds on the other isoform (Fig. 1a).

Enrichment of phage expressing i-bodies binding to recAMA1 was observed after three rounds of panning on either the 3D7 or W2mef antigen (Fig. 1b, c). These phage pools contained i-bodies that bound to recAMA1 of other *P. falciparum* strains (7G8, FVO, HB3 and D10), indicating that the pools contained phage that expressed i-bodies with broad specificity (Supplementary Figs. 1, 2). At each round of cross-panning, there were binders to both the 3D7 and W2mef isoforms of recAMA1, which were used in the original panning campaign. Since these ELISAs were carried out using pooled phage, it was possible that the pools contained many clones that bound to one or other, but not both forms of recAMA1. Forty-eight clones from the last round of each panning campaign were expressed as i-bodies in the periplasm of *E. coli*. ELISA screening of these clones revealed a wide spectrum of binding to the different forms of AMA1. This presumably reflected the level of i-body expression in addition to the binding affinity for a particular form of AMA1 (Fig. 1d). Sanger sequencing of 117 of these positive clones from all panning campaigns identified 12 unique i-body sequences (Fig. 1e).

When 12 i-bodies representing these sequences were tested by ELISA for their binding ability to a range of *Pf*AMA1 isoforms (3D7, W2mef, 7G8, FVO, D10, and HB3), different binding specificities were observed (Fig. 1f). The WD33 and WD34 i-bodies, which were identified exclusively in the cross-panning campaign, bound to all AMA1 isoforms examined, but not to reduced and alkylated AMA1, indicating that these two i-bodies bind to conserved conformational epitopes shared by all isoforms of *Pf*AMA1 (Fig. 1g and Supplementary Fig. 3).

The WD33 and WD34 i-bodies bound to parasite *Pf*AMA1 when used to immunoblot extracts of saponin-lysed schizonts (3D7, W2mef, FVO and 7G8) electrophoresed under non-reducing conditions, but not reducing conditions (Fig. 2a). Both WD33 and WD34 bound specifically to a band of the predicted size for full-length AMA1 and another band corresponding to a processed fragment of AMA1. The identity of both bands was confirmed using well-characterised anti-AMA1 mAbs (Supplementary Fig. 4). The ability of these i-bodies to bind parasite AMA1 was confirmed by indirect immunofluorescence microscopy, which showed both WD33 and WD34 binding to merozoites within segmented schizonts with the expected staining pattern for AMA1 and colocalising with mAb 5G8, an AMA1 pro-domain specific mAb (Fig. 2b). The specificity of WD34 binding to AMA1 was further validated by immunoprecipitation followed by mass spectrometry (Supplementary mass spectrometry data).

WD34 binds to the conserved hydrophobic cleft region of AMA1 with low nanomolar affinity

The ability of anti-AMA1 i-bodies to inhibit the interaction of *Pf*RON2 with *Pf*AMA1 was examined using a biotin-tagged synthetic peptide representing a hairpin loop of *Pf*RON2 that has been shown to bind to AMA1[13,36]. Initial screening revealed a dramatic reduction of RON2 peptide binding to 3D7 recAMA1 in the presence of an equivalent concentration of WD34 (Fig. 3a). The results of a competition ELISA confirmed that WD34 inhibited the binding of the RON2 peptide to AMA1 in a dose-dependent manner (Fig. 3b). None of the other 11 representative i-bodies tested, including WD33, inhibited the interaction of rec*Pf*AMA1 and the *Pf*RON2 peptide, further confirming that the WD33 and WD34 epitopes differ. The binding of the WD33 and WD34 i-bodies to different isoforms of *Pf*AMA1 was characterised by surface plasmon resonance (SPR). WD34 bound to all forms of AMA1 examined, consistent with the initial observations from ELISA, immunoblotting, and indirect IFA experiments, with all binding affinities (K_D) in the low nanomolar range (Fig. 3c). The K_D values of WD34 binding to the six isoforms of *Pf*AMA1 ranged from approximately 1–20 nM with the lowest and highest K_D values observed with 7G8 AMA1 (1.07 ± 0.78 nM) and HB3 AMA1 (19.7 ± 7.9 nM), respectively. In a control experiment, the RON2 peptide bound to *Pf*AMA1 with a K_D similar to previously reported values[36].

To identify whether WD34 binds directly to or at a site close to the conserved hydrophobic cleft involved in RON2 binding, competition ELISAs were performed with two mAbs (1F9 and 4G2) whose epitopes have been previously identified as proximal to the hydrophobic cleft[21,28]. Both mAbs inhibited the binding of WD34 in a dose-dependent manner, although 1F9 appeared to have a greater impact on WD34 binding than 4G2 (Fig. 3d). In contrast, the binding of WD33 was inhibited by mAb 4G2, but not mAb 1F9 (Supplementary Fig. 5). These data suggest that the WD34 epitope lies between the footprints of mAbs 1F9 and 4G2, which are at opposite ends of the conserved hydrophobic cleft in *Pf*AMA1.

WD34 binds to AMA1 from other *Plasmodium* species

As their epitope(s) appeared to be highly conserved, the WD33 and WD34 i-bodies were tested for binding to recAMA1 from two other *Plasmodium* species: *P. vivax* (*Pv*-Palo alto strain), which is the second leading cause of human malaria, and the rodent parasite *P. chabaudi adami* (*Pc*-556KA strain). WD34 bound to both *Pv* and *Pc*AMA1,

https://doi.org/10.1038/s41467-024-50770-7

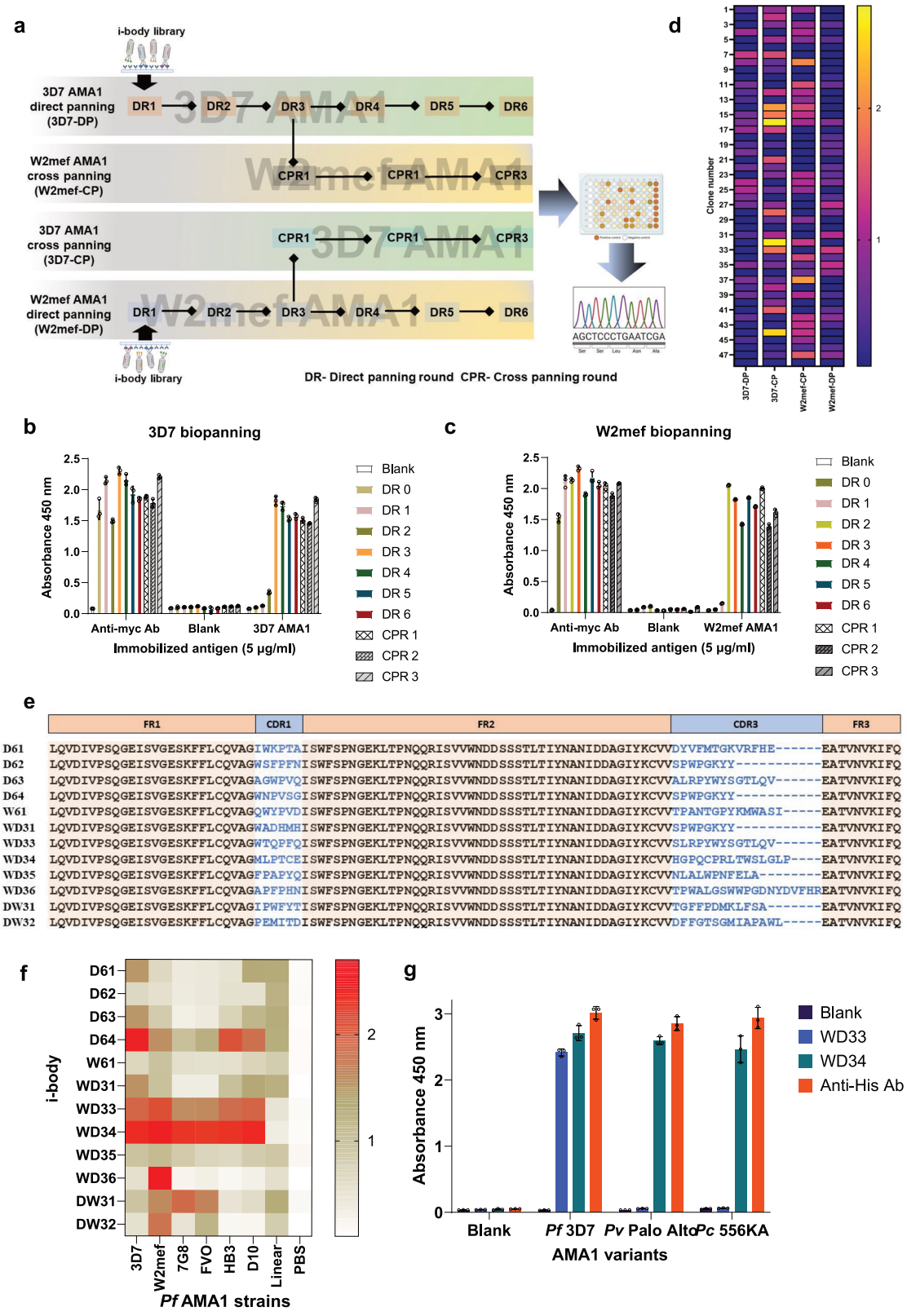

indicating that this epitope is conserved across *Pf* strains and in at least some other *Plasmodium* species (Fig. 1g). In contrast to WD34, WD33 bound to neither *Pv* nor *Pc*AMA1. The affinity of WD34 for *Pv*AMA1 (119 ± 37 nM) and *Pc*AMA1 (26.1 ± 4.1 nM) was approximately 30-fold and 8-fold lower, respectively, than the average K_D value for *Pf*AMA1 isoforms. These data indicate that WD34 binds strongly to many isoforms of *Pf*AMA1 and AMA1 from other *Plasmodium* species despite extensive polymorphic changes in these molecules; it is estimated that approximately 10% of the ectodomain amino acid residues in *Pf* and *Pv*AMA1 are polymorphic[37]. The slight differences in K_D values between the different *Pf*AMA1 isoforms and WD34 could be due to the involvement of some polymorphic residues in the WD34-AMA1 interaction. The affinity of WD33 for *Pf*AMA1 isoforms ranged from 10–20 nM (Fig. 3c). These data indicate that the different abilities of WD34 and

Fig. 1 | Selection of anti-*Pf*AMA1 i-bodies. a Outline of the strategy used for haplotype-distance biopanning the phage-displayed i-body library on 3D7 and W2mef recAMA1. The figure was created with BioRender.com and released under a Creative Commons Attribution-NonCommercial-NoDerivs 4.0 International license. **b** ELISA of phage pools from the biopanning campaign against immobilised 3D7 recAMA1. **c** ELISA of phage pools from the biopanning campaign against immobilised W2mef recAMA1. In both campaigns, three independent experiments were performed as triplicates. Data are presented as mean values ± SD. **d** ELISA screening of individual i-bodies for *Pf*3D7AMA1 binding. Forty-eight clones were randomly selected from each biopanning campaign. i-bodies were expressed in *E. coli* and assessed for AMA1 binding in an ELISA. The binding of the i-bodies to the different AMA1 isoforms is represented as a heat map. Two independent experiments were performed as triplicates. **e** Sequence alignment of AMA1-specific i-bodies with the CDR1 and CDR3 sequences highlighted in blue. **f** Binding profile of i-bodies against *Pf*3D7, W2mef, 7G8, FVO, HB3, D10 recAMA1 isoforms and reduced and alkylated 3D7 AMA1 represented as a heat map where the darker the shade, the greater the binding. Three independent experiments were performed for each i-body. **g** Analysis of WD33 and WD34 binding to *Pv* and *Pc*AMA1. Three independent experiments were performed. Data are presented as mean values ± SD. Source data are provided as a Source Data file.

WD33 to inhibit RON2 binding were not due to differences in binding affinity of the two i-bodies.

AMA1 interacting residues of WD34 are conserved in *Plasmodium*

To understand the structural basis of WD34 binding to AMA1 and its pan-specificity, we determined the crystal structures of WD34 in complex with *Pf* (3D7) recAMA1 and *Pv* (Palo Alto) recAMA1 (both domain I + II) to resolutions of 2.4 Å and 3 Å, respectively (Fig. 4a–c, Supplementary Fig. 6 and Supplementary Table 2). Consistent with previous publications, both *Pf* and *Pv*AMA1 constructs used here adopted the conserved two domain structure previously observed for AMA1[20,21,38–40]. Similarly, WD34 has the typical compact globular structure described for an i-body[29] featuring a series of beta-strands, a canonical disulphide bond in the scaffold, and two loop regions corresponding to CDR1 and CDR3. In both i-body-AMA1 complexes, the WD34 footprint spans the conserved hydrophobic cleft in AMA1, perpendicular to the RON2 peptide footprint (Fig. 4d–f). The AMA1-surface area buried by WD34 is 1645 Å and 1972 Å for *Pf* and *Pv*AMA1, respectively. These buried surface areas are remarkably large, particularly considering that WD34 is a single Ig domain with only two CDRs. Indeed, the observed buried surface areas are larger than the footprints of previously identified invasion inhibitory anti-AMA1 antibodies, including 1F9 (1220 Å in PDB ID: 2Z8V) and IgNAR (14I1-M15) (1205 Å in PDB ID: 2Q8A)[21,40]. In contrast to 1F9 and IgNAR (14I1-M15), which interact with the highly polymorphic loop 1d of AMA1, WD34 binds mainly to relatively conserved residues in AMA1 domain I of both *Plasmodium* species, displaying only minor differences in the two binding interfaces (Fig. 4a, b and Supplementary Figs. 6, 7).

As expected, the CDR1 and CDR3 regions of the i-body are responsible for most of the interactions with AMA1 (Supplementary Table 2). In both complexes, an additional disulphide bond linking CDR1 (C22) and CDR3 (C31) constrains the flexibility of the CDR loops in WD34 (Fig. 4g). This disulphide bond is essential for the interaction of WD34 with AMA1, as mutating C22 and C31 to serine completely abolished the interaction (Fig. 4g). In both complexes, at least 12 of the 21 CDR residues in WD34 are involved in binding to AMA1 (Supplementary Table 2). Apart from interacting with the residues in the CDR3 and CDR1 loops of WD34, AMA1 also interacts with WD34 scaffold residues, forming several direct contacts. A detailed description of this interaction is provided in Supplementary information (Supplementary Fig. 8).

Although the WD34 footprint is nearly identical in size and location in *Pf* and *Pv*AMA1, there are some differences in the i-body-antigen interactions in the two complexes that should be noted. One difference is that WD34 forms more hydrogen bonds with *Pf*AMA1 than with *Pv*AMA1 (Supplementary Table 2). In the WD34-AMA1^{Pf} complex, G80^{WD34} and W88^{WD34} interact with AMA1 via hydrogen bonds, whereas these residues only have weak van der Waals interactions with *Pv*AMA1. Another difference is the mode of engagement with Y234^{Pf} (Y179^{Pv}). In the WD34-AMA1^{Pf} complex W88^{WD34} contacts Y234^{Pf} via a π stacking interaction (Supplementary Fig. 9), which is absent in the WD34-AMA1^{Pv} complex. FoldX position scan software showed that the WD34-AMA1^{Pf} complex exhibits more free binding energy than the WD34-AMA1^{Pv} complex, consistent with the higher binding affinity observed in the SPR analyses[41] (Supplementary Fig. 10). This detailed structural information provides a molecular explanation for the observation that WD34 binds to AMA1 from these two major human *Plasmodium* species and does so with slightly different affinities.

WD34 inhibits erythrocyte invasion by merozoites of multiple *Plasmodium* species

The inhibitory activity of WD33 and WD34 on parasite growth was tested using in vitro parasite growth inhibition assays. WD34, but not WD33 inhibited all the *P. falciparum* strains tested (3D7, W2mef, 7G8 and Dd2) with the mean half-maximal inhibitory concentration (IC_{50}) ranging from 13 µg/ml to 40 µg/ml (Fig. 5a–c). *P. vivax* cannot be maintained in continuous culture to study invasion. Because of this, we used a transgenic *P. falciparum* line engineered to express *Pv*AMA1. In addition, *P. knowlesi*, which can be cultured in vitro, was also examined. WD34 inhibited the growth of both the *Pf*3D7 transgenic *Pv*AMA1 parasite line and *P. knowlesi* parasites in a dose-dependent manner, with IC_{50}S of 84 µg/ml and 128 µg/ml, respectively. The broadly similar potency of WD34 in inhibiting multiple parasite lines is consistent with the structural and functional data described above. Importantly, the IC_{50} values for WD34 reported here are lower than previously published values for AMA1 antibodies that inhibit merozoite invasion[42,43].

WD34 inhibits hepatocyte invasion by sporozoites of *P. falciparum*

Previous reports have indicated that the AMA1-RON2 complex is involved in hepatocyte invasion by sporozoites[14,15,44]. To investigate the effect of WD34 on cell traversal, salivary gland sporozoites of the *Pf*NF54 strain were incubated with HC-04 hepatocytes in the presence of fluorescein isothiocyanate (FITC)-dextran and increasing concentrations of WD34. WD34 did not significantly inhibit hepatocyte traversal when compared to the negative control i-body, 21H5, although there was some modest inhibition at the highest WD34 concentration tested (Fig. 5d). This finding, with *P. falciparum* sporozoites aligns with the recent observation made by Fernandes et al.[15] that conditional loss of AMA1 and RON2 did not affect *P. berghei* sporozoite migration.

To test the effect of WD34 on parasite invasion of hepatocytes, sporozoites of *Pf*NF54 were incubated with HC-04 cells in the presence of the i-body, and the number of cells containing CSP-positive intracellular parasites was quantified using flow cytometry 24 h after the treatment. Hepatocyte invasion by NF54 was moderately inhibited by WD34 in a dose-dependent manner (mean difference 62.9%; $p = 0.0178$), but NF54 was not significantly affected by the control i-body (mean difference 35.1%; $p \geq 0.4006$) (Fig. 5e). These results are consistent with the AMA1-RON2 interaction being important for *P. falciparum* sporozoite invasion of hepatocytes[14,15,44].

WD34 has a short suppressive effect on *P. berghei* infections in mice

To assess whether WD34 has an effect on *P. berghei* parasitaemia in mice, we performed a Peters' 4-day suppressive test[45] using BALB/c mice. Treatment of mice once daily with WD34 (30 mg/kg, I.P.) for

https://doi.org/10.1038/s41467-024-50770-7

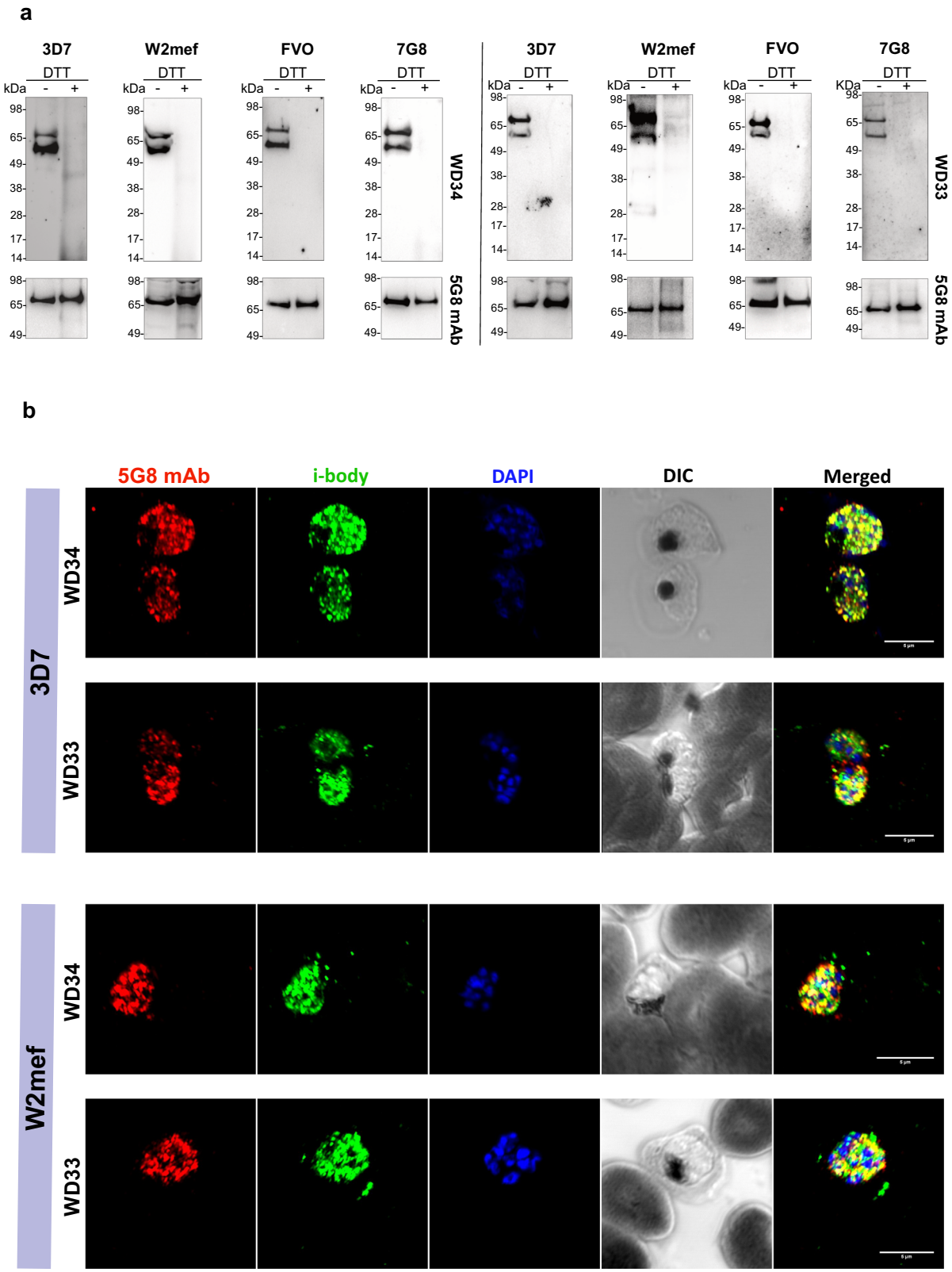

Fig. 2 | WD33 and WD34 recognise AMA1 expressed by *P. falciparum*. **a** Immunoblotting of saponin-lysed *Pf*3D7, W2mef, FVO and 7G8 schizonts. Parasite material was fractionated by SDS-PAGE under reducing or non-reducing conditions. After transfer, membranes were probed with either WD34 or WD33 and then HRP-conjugated anti-myc mAb 9E10. mAb 5G8, which binds a linear epitope near the N-terminus of AMA1, was used as a control (lower panel). At least two independent experiments were performed. Source data are provided as a Source Data file. **b** Indirect immunofluorescence of fixed 3D7 and W2mef schizonts with pro-domain specific mAb 5G8, and i-bodies WD33 and WD34. At least two independent experiments were performed.

https://doi.org/10.1038/s41467-024-50770-7

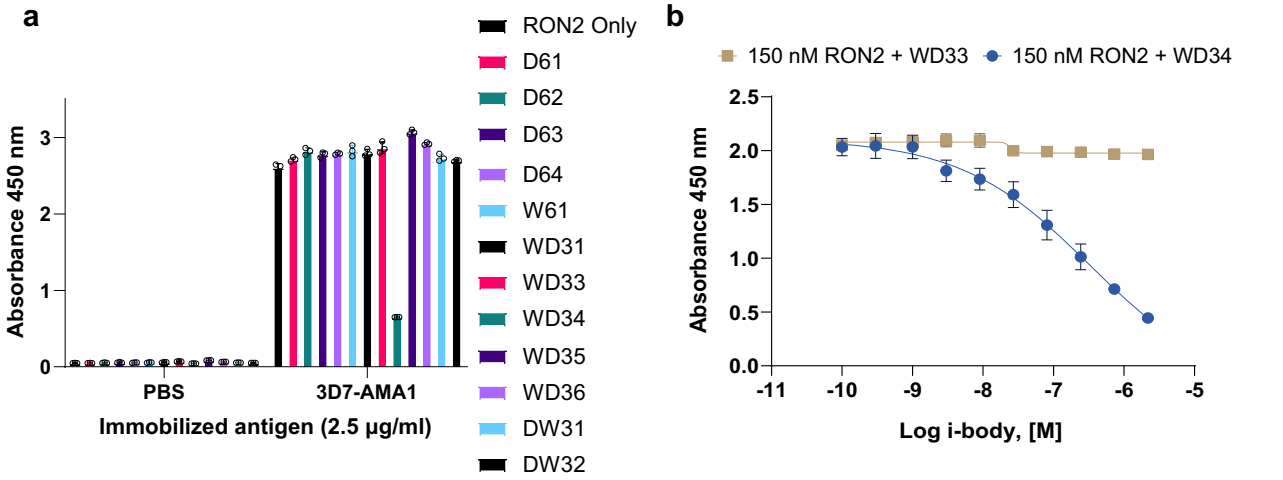

c

AMA1 Variant		K_D(nM)		
		RON2 peptide	WD34	WD33
P. falciparum	3D7	22.3(±3.94)	7.16(±3.54)	19.3(±1.44)
	W2mef	12.3(±1.92)	4.90(±5.71)	16.8(±1.61)
	FVO	6.31(±0.48)	1.96(±0.30)	11.4(±1.11)
	7G8	5.16(±0.65)	1.07(±0.78)	21.3(± 1.81)
	HB3	7.54(±1.07)	19.7(±6.2)	18.6(± 2.25)
	D10	15.9(±1.33)	3.78(±2.01)	16.4(±2.05)
P. vivax	Palo Alto	No binding	119 (±37.3)	No binding
P. chabaudi	556KA	No binding	26.1(±14)	No binding

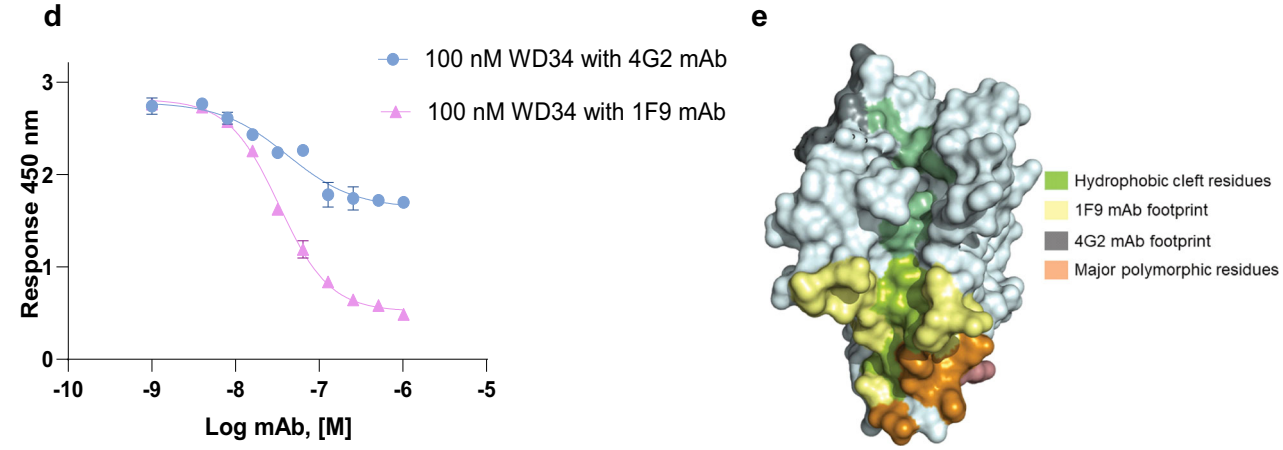

Fig. 3 | Characterisation of the WD33 and WD34 interactions with AMA1. a ELISA showing the binding of biotinylated RON2 peptide (150 nM) to immobilised AMA1 in the presence of i-body (150 nM). AMA1-bound RON2 peptide was measured using streptavidin HRP. Data are presented as mean values ± SD. **b** Inhibition of RON2 peptide (150 nM) binding to AMA1 by increasing concentrations of WD34. Data are presented as mean values ± SD. Source data are provided as a Source Data file. **c** Equilibrium dissociation constants (K_D) of WD34 and WD33 interacting with AMA1 determined by surface plasmon resonance. All the generated sensorgrams were analysed by T200 evaluation software. At least three independent experiments were performed to get the final reported values. K_D values are reported at the nanomolar level, and the standard deviations are reported in parenthesis. See the Supplementary SPR information. **d** Dose-dependent inhibition of WD34 binding to AMA1 by mAbs 1F9 and 4G2, which have been previously reported to bind around the hydrophobic cleft (**e**). Three independent experiments were performed. Data are presented as mean values ± SD.

https://doi.org/10.1038/s41467-024-50770-7

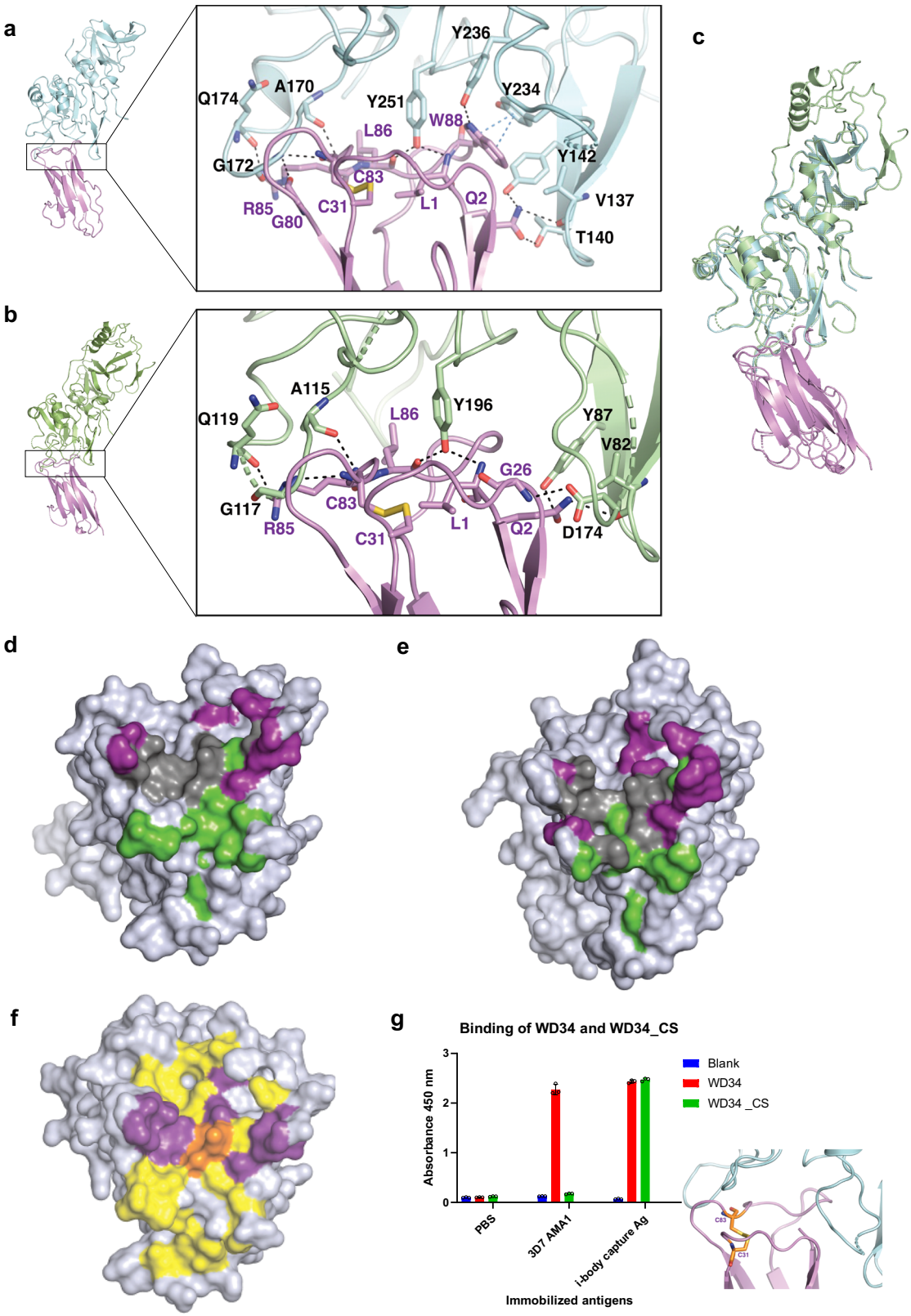

Fig. 4 | Structural analyses of WD34-AMA1 complexes. a Crystal structure of the WD34-AMA1^{Pf} complex. *Pf* AMA1 is in cyan, and WD34 is in purple. **b** Crystal structure of the WD34-AMA1^{Pv} complex. *Pv*AMA1 is shown in green, and WD34 is shown in purple. **c** Superimposition of the WD34-AMA1^{Pf} and WD34-AMA1^{Pv} complexes. **d** WD34 footprint (purple) on *Pf*AMA1 compared to the hydrophobic cleft (green). The shared footprint is shown in grey. **e** WD34 footprint (purple) on *Pv*AMA1 compared to the hydrophobic cleft (green). **f** WD34 footprint (purple) compared to the *Pf*RON2 peptide footprint (yellow). The shared region is depicted in orange. **g** ELISA showing that the WD34CS mutant, in which C22^{WD34} and C31^{WD34} were mutated to serine failed to bind to *Pf*AMA1. Three independent experiments were performed, and data are presented as mean values ± SD. Source data are provided as a Source Data file.

https://doi.org/10.1038/s41467-024-50770-7

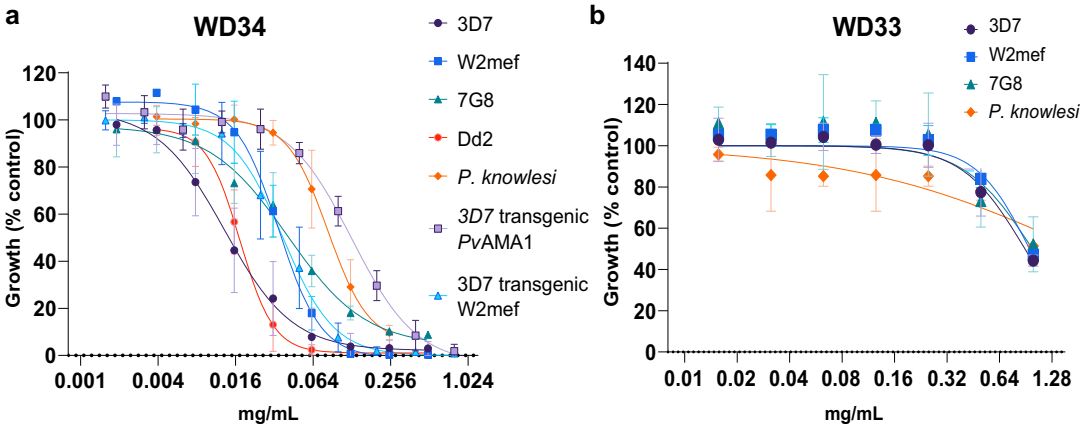

c

IC50 Values

Parasite line	WD34 mg/mL	WD34 µM	WD33 mg/mL	WD33 µM
P. falciparum				
3D7	0.01	0.95	0.89	63.91
W2mef	0.03	2.49	0.95	67.90
7G8	0.04	2.92	0.98	70.53
Dd2	0.02	1.24	ND	ND
P. knowlesi	0.08	6.01	1.81	129.36
3D7 transgenic *Pv*AMA1	0.12	9.21	ND	ND
3D7 transgenic W2mef	0.03	2.68	ND	ND

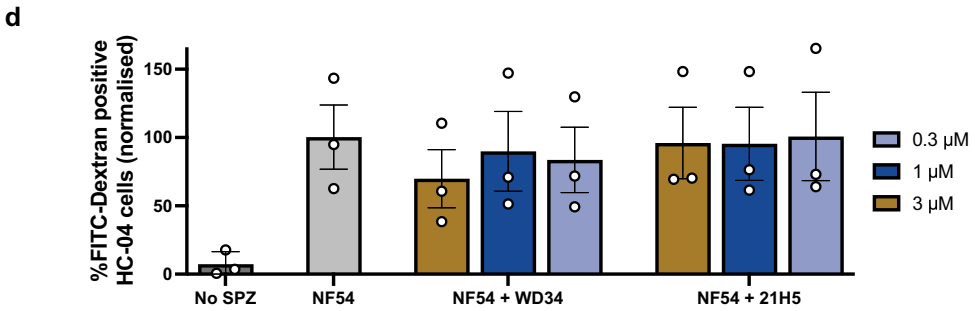

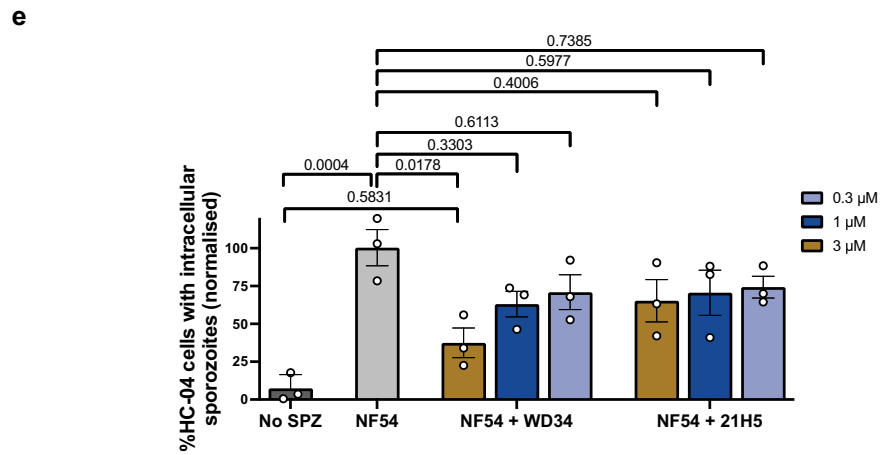

4 days suppressed parasitaemia at day 4 by approximately 49% compared to untreated mice ($p = 0.0294$) (Fig. 6b, c). However, this suppressive effect was short-lived, persisting for no more than 2–3 days, after which the parasitaemia rapidly rose to the levels seen in untreated mice, with all animals succumbing to malaria by day 9 ($p = 0.2124$). It is possible that this transient effect was due to either poor serum stability or the short half-life of WD34. Therefore, we examined the thermal stability, serum stability and pharmacokinetic profile of WD34. In these experiments, WD34 was stable in both PBS and mouse serum (Supplementary Fig. 14) but had a very short half-life (Supplementary mass spectrometry information). Immunoblotting of *P. berghei*-infected erythrocytes demonstrated that WD34 specifically recognised *P. berghei* AMA1, with a single ~55 kDa band detected in infected cells, but not in uninfected cells. Under reducing conditions, the *P. berghei*-

Fig. 5 | WD34 inhibits both merozoite and sporozoite life-cycle stages. **a** Inhibition of merozoite growth by WD34 was tested using multiple *Plasmodium* parasites. Assays were performed using two-fold dilutions of WD34 starting with 0.5 mg/ml. Data represents the mean of three independent experiments and error bars represent standard deviations. **b** Growth inhibition of multiple *Plasmodium* parasites by WD33. Assays were performed with two-fold dilutions of WD33 starting with 1 mg/ml. Three independent experiments were performed, and data points are represented as mean values ± SD. **c** IC_{50} values for each parasite line were calculated by using the non-linear regression model. **d**, **e** Effect of i-bodies on sporozoite traversal (**d**) invasion (**e**) of HC-04 hepatocytes by *P. falciparum* sporozoites. WD34 or 21H5 treated FITC-Dextran+HC-04 cells or HC-04 cells were incubated with sporozoites. Cell traversal and invasion were measured at 3 and 24 h, respectively. The mean of $n = 3$ biological triplicates and standard deviations (**a**, **b**) or standard errors of the mean (**d**, **e**) are shown. Statistical analysis: 2-way ANOVA with multiple comparisons. Source data are provided as a Source Data file.

specific i-body signal was drastically reduced, suggesting WD34 recognised a disulphide bond-dependent epitope in *Pb*AMA1 (Fig. 6f). Taken together, these data demonstrate that WD34 has a short suppressive effect on *P. berghei* growth in vivo.

Discussion

AMA1 has been studied extensively as a potential component of a vaccine against *P. falciparum* and *P. vivax* malaria. However, like most *P. falciparum* merozoite proteins that are natural immunogens, AMA1 is highly polymorphic, and this has prevented the generation of broadly protective immune responses in field trials with AMA1-containing vaccines[23,46–48]. Here, we used an i-body (WD34) isolated from a phage-display library to identify a previously unrecognised highly conserved epitope in AMA1. To isolate WD34 and other cross-reactive i-bodies, we used a cross-panning strategy on *Pf*3D7 and *Pf*W2mef recAMA1, which were chosen because of their extensive sequence differences[33]. In contrast to the cross-reactive characteristics of the i-bodies selected using the cross-panning strategy, i-bodies selected by direct panning on one or other of the recAMA1 isoforms were more strain-specific.

WD34 reacted strongly with both isoforms of AMA1 used in the cross-panning strategy to select this i-body and with four other isoforms of *Pf*AMA1 examined. Unexpectedly, WD34 cross-reacted with AMA1 of *P. vivax* (Palo Alto strain), the other major cause of human malaria, with AMA1 of *P. knowlesi*, which causes malaria in humans and other primates, and AMA1 of the rodent parasite, *P. chabaudi adami* (556KA strain).

Using rec*Pf*AMA1 and a synthetic peptide representing the extracellular loop of *Pf*RON2, we showed that WD34 blocked the interaction between AMA1 and its ligand, which is inserted by the parasite into the erythrocyte cell membrane prior to merozoite invasion. As WD34 also blocked the binding of mAbs 1F9 and 4G2, whose epitopes lie at opposite ends of the RON2-binding cleft, we concluded that the WD34 epitope lies in the central region of this hydrophobic cleft. This was confirmed by solving the X-ray crystal structures of the WD34-AMA1^{Pf} and WD34-AMA1^{Pv} complexes to resolutions of 2.4 Å and 3 Å, respectively. The WD34 footprint consisted of relatively conserved residues in the central region of the RON2-binding cleft of both the *Pf* and *Pv* isoforms of AMA1, distant from the highly polymorphic loop 1d in *P. falciparum*, which is targeted by the "strain-specific" mAb, 1F9[21].

In both complexes, WD34 contacts a small number of residues in the hydrophobic cleft that are directly involved in RON2 binding, but most of the WD34 contacts are with surrounding residues on both sides of the cleft in loops 1a, 1b, 1c and 1e[20] (Supplementary Fig. 11). Notably, of the six WD34 contact residues common to *Pf* and *Pv*AMA1, five are strictly conserved in AMA1 of all isolates of multiple *Plasmodium* species collected in multiple countries where malaria is endemic. Only one residue (G172) is clearly polymorphic (Fig. 7). In ~32% of the *Pf*AMA1 sequences surveyed and in the HB3 isoform studied here, G172, which makes contacts with G80^{WD34}, is mutated to glutamic acid (Fig. 7 and Supplementary Fig. 12). This difference may be responsible for the WD34 binding affinity for HB3 *Pf*AMA1 (K_D = 19.7 nM) being slightly lower than for the other five *Pf*AMA1 isoforms studied (K_D = 1.07–7.16 nM). In <1% of *Pf* parasites surveyed, this residue was mutated to either valine or arginine, but the effect of these mutations on WD34 binding affinity was not examined (Supplementary Fig. 12). Furthermore, there is a high conservation of WD34-AMA1^{Pf} contact residues in AMA1 of the rodent parasite *P. chabaudi*, which had a similar low nanomolar binding affinity in SPR analyses (Supplementary Fig. 12c). The finding that the binding affinity of WD34 for *Pv*AMA1 was approximately 30-fold less than its binding affinity for *Pf*AMA1 is not surprising given that WD34 was selected by panning the i-body-phage library on *Pf*3D7 AMA1. Although there are many conserved features to the WD34 epitope in these two forms of AMA1, there are also differences in the two interfaces, which could account for this difference in binding affinity. Notably, WD34 forms more polar interactions with *Pf*AMA1 than with *Pv*AMA1 (Supplementary Table 2). For example, G80 and W88 of WD34 form hydrogen bonds to *Pf*AMA1 G172 (3.2 Å) and 2.82 Å Y236 (2.82 Å), respectively, but equivalent interactions are lacking in the WD34-AMA1^{Pv} complex.

A characteristic property of camelid nanobodies or shark single-domain antibodies (VNARs) is their ability to interact via their extended CDR3 loops with concave epitopes not accessible to conventional antibodies[49]. The WD34 i-body studied here also has an extended CDR3 loop, but rather than penetrating the hydrophobic RON2-binding cleft of AMA1 like the IgNAR (14I1-M15), the CDR3 and CDR1 loops, with some framework residues, form a paratope that spans the RON2-binding cleft[40]. Despite the small size of the i-body compared to conventional antibodies, the WD34 footprint is considerably larger than that of previously characterised anti-AMA1 antibodies[21,40]. This may, at least partly, be due to the disulphide bond between CDR1 and CDR3 facilitating a spatial arrangement of the CDR loops that provides a flattened paratope surface. An important consequence of the large interface between WD34 and the surface of AMA1 may be a tolerance of polymorphisms, contributing to the broad cross-reactivity described here.

The binding of *Pf*AMA1 to a hairpin loop of *Pf*RON2 is important for the invasion of host cells by merozoites and sporozoites[11–16,50,51]. Although there is evidence suggesting that *Pf*AMA1 and *Pv*AMA1 may have another binding interaction in addition to the RON2-loop interaction[52], it was notable that the WD34 i-body inhibited the invasion of erythrocytes and hepatocytes by *P. falciparum* merozoites and sporozoites, respectively[53]. The inhibitory potency of WD34 in merozoite growth inhibition assays was broadly similar for multiple strains of *P. falciparum* and for *P. knowlesi*, with the IC_{50} values reported here being some of the lowest for an "antibody" recognising multiple parasite lines. To our knowledge, this is the first time a cross-species anti-AMA1 antibody-like molecule with potent invasion inhibitory properties has been reported. Previously, Collins et al.[28] and Igonet et al.[27] described two AMA1 mAbs with broad strain and species specificity, however, both these mAbs showed rather poor in vitro inhibitory activity[27,43,54]. Furthermore, antibodies to other *Plasmodium* antigens having similar potent inhibitory activity and broad strain and species specificity have not been reported.

In a preliminary in vivo study, WD34 suppressed parasitaemias in mice by 50% 4 days after challenge with *P. berghei*. However, this effect was short-lived, and parasitaemias returned to control levels shortly after the last WD34 treatment. Pharmacokinetic and serum stability studies indicated that the transient effect observed is primarily attributed to the short half-life resulting from rapid renal clearance, which aligns with the smaller molecular weight of WD34. These results supported the previously published pharmacokinetic data for another

https://doi.org/10.1038/s41467-024-50770-7

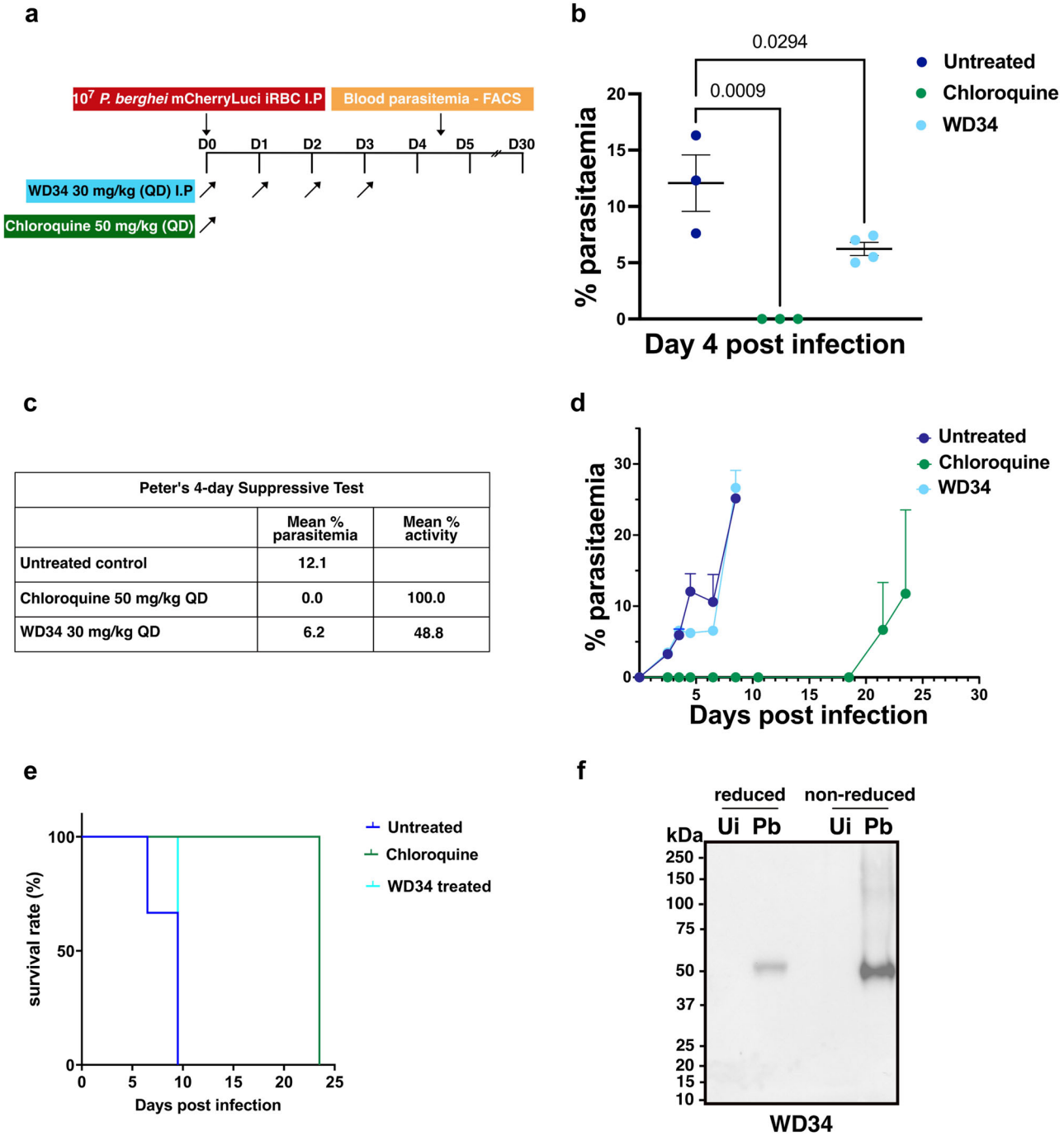

Peter's 4-day Suppressive Test		
	Mean % parasitemia	Mean % activity
Untreated control	12.1	
Chloroquine 50 mg/kg QD	0.0	100.0
WD34 30 mg/kg QD	6.2	48.8

Fig. 6 | WD34 suppression of *P. berghei* parasitaemias in BALB/c mice. **a** Experimental design and WD34 treatment schedule ($n = 3$ for untreated controls, $n = 3$ for chloroquine-treated controls, and $n = 4$ for WD34 treatment). Treatments were given once daily (Q.D). One experiment was performed. **b** Level of suppression of *P. berghei* infections by WD34. Data are represented as means ± SEM. Statistical analysis: 1-way ANOVA with multiple comparisons. **c** In vivo efficacy of WD34 against *P. berghei* infections using Peters' 4-day suppressive test. **d** Development of parasitaemias in untreated control mice, chloroquine-treated control mice, and WD34-treated mice. Recrudescences were seen with chloroquine due to giving a single dose on day 0. Data are presented as mean values ± SD. Source data are provided as a Source Data file. **e** Survival of WD34-treated mice was similar to untreated control mice. **f** Immunoblot with WD34 of uninfected erythrocytes (Ui) and erythrocytes infected with *P. berghei* expressing mCherry-luciferase (*Pb*) under reducing and non-reducing conditions. At least two independent experiments were performed.

i-body (AD-114), where the serum half-life was estimated to be 11 min[55]. That study showed that PEGylation dramatically extended the half-life of the i-body. In view of these results, in vivo half-life extension for WD34 will be explored in future.

Malaria vaccine development has made important advances in the last decade with two vaccines targeting *P. falciparum* sporozoites now approved for use[56–59]. As discussed earlier, the polymorphisms in AMA1 have proven to be a major barrier to efforts aimed at developing a vaccine incorporating this asexual blood-stage antigen. One approach to overcoming this problem has been to immunise with an AMA1-RON2 complex. This approach has shown promise in preclinical studies and has demonstrated that there are conserved or less antigenically diverse epitopes in AMA1 that can be targeted by protective antibodies[60–62]. However, it is not yet clear whether the highly

https://doi.org/10.1038/s41467-024-50770-7

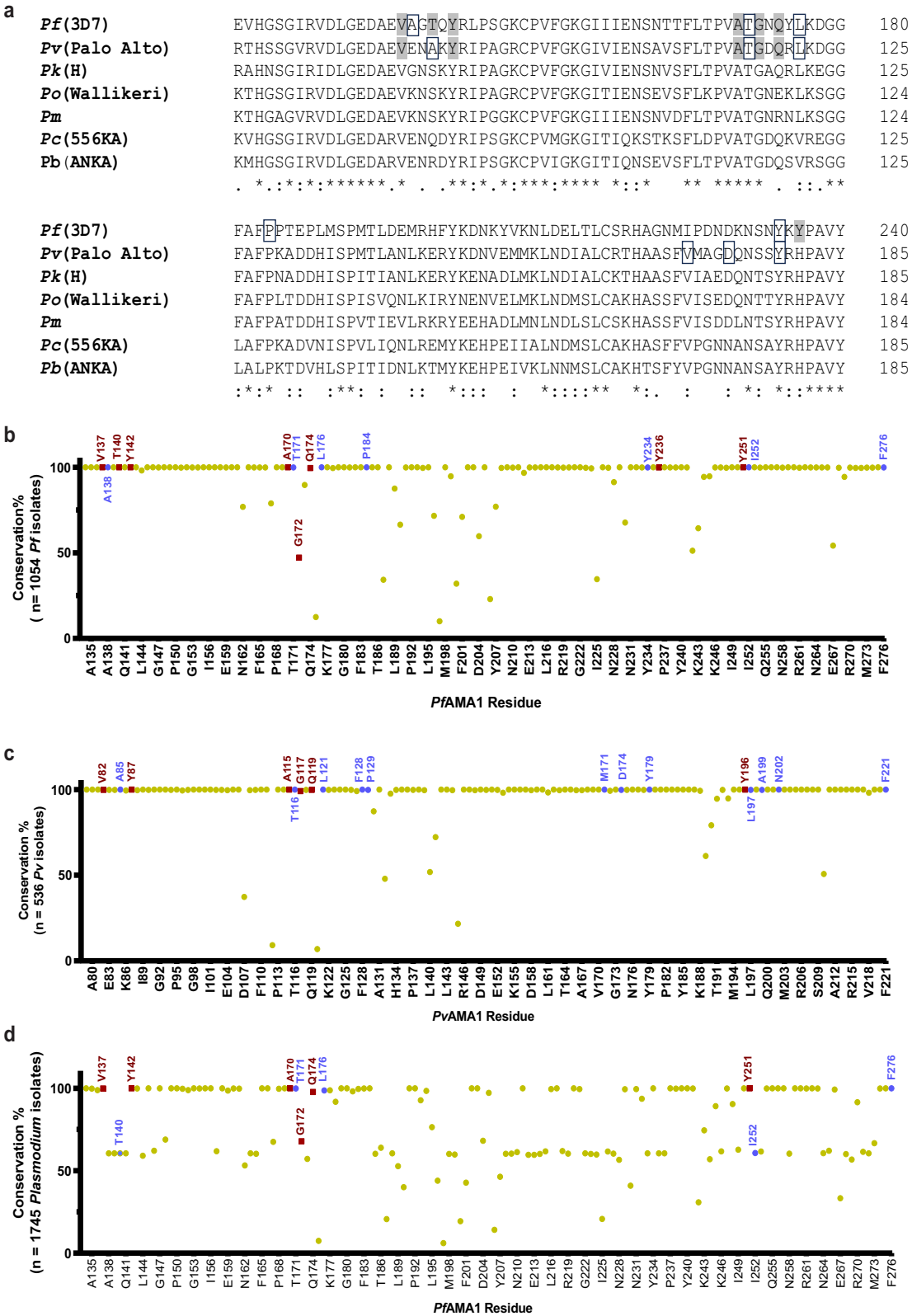

Fig. 7 | Conservation of residues in *Plasmodium* AMA1 that interact with WD34. **a** Alignment of AMA1 sequences of multiple *Plasmodium* species showing conservation of WD34 contact residues (<4 Å) identified in the *Pf* and *Pv* AMA1-WD34 complexes. Polar interactions are shown in grey boxes and van der Waals bonds are shown in open boxes. **b**–**d** Percentage conservation of WD34 contact residues in AMA1 of multiple isolates: **b** *P. falciparum* (1054 sequences); **c** *P. vivax* (586 sequences); and **d** *Plasmodium* species (1745 sequences). Polar interactions are shown in red and van der Waals interactions are shown in blue. A detailed analysis is provided in Supplementary Fig. 12 and Supplementary Data 1.

conserved WD34 epitope described here can be targeted by a natural antibody response or antibodies induced by vaccination. If a form of AMA1 can be engineered that diverts the induced antibody response away from highly polymorphic regions, such as loop 1d, towards relatively conserved regions, such as the WD34 footprint defined here, AMA1 may have renewed potential as a vaccine candidate, especially given the possibility of using this approach for both *P. falciparum* and *P. vivax* malaria[25]. However, it is possible that the WD34 epitope is poorly immunogenic, and its identification here may have resulted from the use of the large naive i-body library in which the range of CDR sequences was not restricted by immunisation or infection, which usually proceeds the creation of nanobody or mAb libraries. Whether the WD34 epitope is immunogenic needs to be investigated in future studies to further inform vaccine strategies.

In recent years, evidence has accumulated showing that the control of malaria with drugs and a vaccine may be complemented by using human mAbs to prevent malaria[63–65]. The human mAb, CIS43LS, which targets *Pf*CSP, protected human volunteers *against P. falciparum* infection in both experimental challenge and natural exposure settings[64,66]. Although the major focus of current immunoprophylaxis research has been the *P. falciparum* CSP antigen, antibodies targeting asexual blood-stage antigens should be considered as a complementary strategy[67]. AMA1 is an attractive candidate for this approach as it is expressed in both pre-erythrocytic and asexual blood stages of the parasite life cycle and present in all *Plasmodium* species infecting humans. The WD34 i-body in its current small, single-domain form is not a candidate for assessment as an immunotherapeutic because of its short half-life. However, it did provide some suppression of *P. berghei* parasitaemia in mice and extending its half-life, for example, with an Fc tag could provide an attractive format for development as an immunoprophylactic agent against multiple species of malaria. A similar strategy has been effective in other fields. AD-214, an i-body with a human IgG Fc against idiopathic pulmonary fibrosis has been shown to be safe and well tolerated in a human Phase 1 safety and tolerability study in healthy volunteers (ClinicalTrials.gov: NCT04415671). This suggests a potential future pathway for a WD34-derived antibody-based therapeutic against malaria.

Methods

Mammalian cells, parasite cultures, peptides, and antibodies

Expi293 and ExpiCHO (ThermoFisher) cells were maintained in Expi293 and ExpiCHO expression mediums (ThermoFisher) at 37 °C, 8% CO_2, 125 rpm. *Plasmodium falciparum* 3D7, DD2, 7G8, FVO and W2mef and *P. knowlesi* parasites were maintained in in vitro cultures at 37 °C according to previously published protocols[68,69]. Biotin-tagged and untagged RON2 peptide (DITQQAKDIGAGPVASCFTTRMS PPQQICLNSVVNTALSTSTQSAMK) with cyclised cysteines were synthesised by Mimotopes, Australia.

mAbs 4G2, 1F9 and 5G8 were obtained from Robin Anders. Anti-c-myc mAb 9E10 and anti-i-body scaffold mAb 7G4 were made at the WEHI Antibody Facility, Bundoora, Australia. Fluorophore and HRP-conjugated Abs were used as follows: Anti-M13 HRP mAb (Catalogue no: 11973-MM05T-H, Sino Biological), anti-His HRP mAb (Catalogue no: A7058, Sigma-Aldrich), goat anti-human IgG (Fc-specific) HRP (Catalogue no: A0170, Sigma-Aldrich), goat anti-mouse IgG (Catalogue no: AP127P, Sigma-Aldrich), Streptavidin HRP (Catalogue no: 21130, ThermoFisher), goat anti-human Alexa fluor 488 (Catalogue no: H10120, Invitrogen), goat anti-rabbit Alexa Fluor 568 (Catalogue no: A11036, Molecular Probes), goat anti-rabbit 546 (Catalogue no: A11081, Invitrogen), goat anti-mouse 568 (Catalogue no: A11031, Invitrogen), goat anti-mouse FITC (Catalogue no: F0257, Sigma-Aldrich).

Expression and purification of recombinant AMA1

Codon-optimised full ectodomain (domain I, II and III) and domain I + II (for X-ray structure determination experiments) sequences of *Pf*3D7, W2mef, 7G8, FVO, HB3, D10 and *Pc*AMA1 were cloned into pET-28a (+)-Tev vector (Genscript, Singapore). AMA1 protein was expressed in inclusion bodies, purified and refolded according to standard protocols[20,70]. The codon-optimised *Pv*AMA1 (Palo Alto) sequence in PcDNA3.1 was kindly provided by James Beeson, Burnet Institute. *Pv*AMA1 was expressed in Expi293 cells and purified from the Expi293 expression medium using Ni-NTA chromatography[50].

Biopanning using the phage-displayed i-body library

Phage panning was performed as described previously with some modifications[29,40]. Phage-displayed i-body library (~10^{10} random i-body sequences cloned into pADL-23c phagemid vector) was amplified in *E. coli* TG1 cells. At OD_{600} = 0.4–0.5, *E. coli* TG1 cells were infected with M13K07 helper phage (Antibody Design Laboratories, USA) to display the i-bodies on phage particles. The amplified i-body phage library was biopanned independently on immobilised recombinant *Pf*3D7 and *Pf*W2mef AMA1 (2.5 μg/ml). Six biopanning rounds were carried out in each biopanning campaign. For cross-biopanning, a portion of the round three phage from each panning campaign was incubated with immobilised recombinant AMA1 of the other isoform (from *Pf*3D7 enriched phage to *Pf*W2mef AMA1 and vice versa). These then underwent a further three rounds of biopanning.

Phage enrichment ELISA, single clone screening and sequencing

Phage ELISAs were performed as described previously[29]. Briefly, 96-well plates (Nunc, Maxisorp) were coated with the antigens and blocked with 5% skim milk. Amplified phage pools of biopanning rounds or single clone phage were incubated at a 1:10 dilution against immobilised antigens. The wells were washed three times with 0.1% PBST, and bound phage were detected with anti-M13 HRP mAb (Sino-biologicals) followed by 3,3′,5,5′-tetramethylbenzidine (ThermoFisher) as enzyme substrate. The enzyme reaction was stopped with 0.1 M HCl, and absorbance was measured at 450 nm.

Phage-infected TG1 single colonies were grown as 2 ml cultures in 48 deep-well plates (Corning Axygen) and induced with 1 mM IPTG for 16 h. The level of i-body expression and AMA1 binding of periplasmic extracts for each clone were assessed by ELISA. The positive clones for both i-body expression and AMA1 binding were sequenced by Sanger sequencing at the Australian Genome Research Facility, Melbourne, Australia.

Expression and purification of i-bodies

AMA1-specific i-body sequences in pADL-23c vector plasmids (Antibody Design Laboratories, USA) were transformed into *E. coli* BL21 cells. Cultures grown overnight at 37 °C in 2YT media supplemented with 0.1% (w/v) glucose and ampicillin (100 μg/ml) were diluted to OD_{600} of 0.1 and incubated at 37 °C. At OD_{600} = 0.7, cells were induced with 1 mM IPTG and subjected to further growth overnight at 28 °C. Periplasmic extraction of the i-bodies was conducted as described previously[71]. Briefly, the centrifuged cell pellets were resuspended in full-strength spheroplast buffer with lysozyme (40 μg/ml) and incubated on ice for 10 min followed by incubation in half-strength spheroplast buffer. The periplasmic fraction was isolated by centrifugation, and i-bodies were purified using immobilised metal affinity chromatography (IMAC) followed by anion exchange (Cytiva-CaptoQ) and size-exclusion chromatography.

Sequences of Human IgG1 Fc region-tagged WD33 and WD34 were designed by cloning into a PcDNA3.1 vector (Genscript, Singapore) to express i-body Fc versions in Expi293 and ExpiCHO (Invitrogen, USA) expression systems. Fc-tagged i-bodies were purified using affinity purification (Mabselect PrismA-Cytiva) and size-exclusion chromatography.

Standard and competition ELISAs

Indirect i-body binding ELISAs were used to determine the specificity of AMA-1-specific i-bodies. All incubations were performed at 100 μl per well at room temperature for 1 h or overnight at 4 °C. Washing

steps included at least three washes with 0.1% PBS-Tween. The screen of i-bodies with the ability to block the RON2 peptide was performed by incubating the same concentrations (50 nM) of biotin-tagged RON2 peptide and i-body against immobilised *Pf*3D7 AMA1 (2.5 μg/ml) and measuring the bound RON2 peptide by using streptavidin HRP.

In competition ELISAs, 150 nM of the biotin-tagged RON2 peptide and increasing concentrations of WD34 and WD33 were incubated in wells coated with 2.5 μg/ml *Pf*3D7 AMA1. Bound RON2 peptide was measured using streptavidin HRP.

Competition ELISAs of WD34 with mAbs 1F9 and 4G2 were performed with 100 nM of human Fc-tagged i-body (WD33 or WD34) and increasing concentrations of mAbs. This mixture of mAb and i-body was added to wells coated with *Pf*3D7 AMA1. Bound WD34 was measured using goat anti-human Fc-specific HRP antibody.

Immunoblotting and immunofluorescence of recombinant proteins and parasites

Late-stage schizonts of *P. falciparum* were purified by using MACS magnetic columns (Miltenyi Biotec) and saponin lysis. Isolated schizonts were lysed with sample buffer and subjected to SDS-PAGE on 4–12% acrylamide gels (BOLT, Invitrogen). *Plasmodium berghei*-infected and uninfected murine erythrocytes were collected from BALB/c mice, and saponin pellets were solubilised in reducing or non-reducing sample buffer prior to equal sample loading and SDS-PAGE through 10% Bis-Tris gels. Proteins were transferred to nitrocellulose membrane for 7 min (iBlot2, Invitrogen) or for 60 min in SDS-PAGE transfer buffer (*P. berghei* blots), blocked with 10% skim milk and probed with 25 μg/ml of i-bodies (in 5% skim milk). Membranes were then washed three times with 0.05% PBST and incubated with anti-myc or HRP (1:5000) secondary antibodies for 1 h before washing and development of membranes. Western blots were developed with West Pico PLUS chemiluminescent reagents (ThermoFisher, USA) and visualised using the Biorad GelDoc or ChemiDoc system.

For fixed immunofluorescence imaging, smears of synchronised late-stage schizonts on glass microscope slides were fixed with 100% methanol for 2 min and incubated in a blocking buffer (4% BSA in PBS) for at least 1 h. i-bodies (10 μg/ml), and fluorophore-tagged secondary antibodies (1:1000) were used. Labelled parasites were imaged with a Zeiss LSM 880 inverted microscope with ×63/1.4 oil objective, appropriate excitations, and an Airyscan detector. Captured images were analysed with ImageJ software.

Immunoprecipitation and mass spectrometry analysis

Late-stage *Pf* (3D7) schizonts were purified by saponin lysis and washed with PBS (pH 7.4) three times. Schizont pellets were lysed by RIPA buffer (Thermo Scientific) according to the manufacturer's protocol. Parasite lysates (100 μl) were incubated with 50 μg of WD34 and 21H5 i-bodies at room temperature for 2 h. Parasite lysate and i-body mixtures were incubated with anti-c-myc Magnetic Beads (Thermo Scientific) overnight, which were then washed with 0.001% PBS-Tween (pH 7.4) five times and PBS (pH 7.4) five times. On-bead tryptic digestion was performed for LC-MS/MS analysis of bound proteins as previously described with minor modifications[72]. Briefly, beads were washed with 20 mM NH_4HCO_3 (pH 8.0) three times and denatured in 8 M urea. Proteins were reduced and alkylated with 2 mM tris-2-carboxyethyl-phosphine and iodoacetamide. Each bead sample was diluted with 800 μl of 50 mM Tris HCl (pH 8.3) and subjected to tryptic digestion (1:100 ratio with antibody load) overnight at 37 °C. Tryptic peptides were recovered, desalted and concentrated according to the published protocol[72].

The tryptic peptides were separated on Ultimate 3000 RSLCnano UHPLC (Thermo Scientific) and analysed on a Q-Exactive HF Orbitrap LC-MS/MS system (Thermo Scientific). The mass-spectral database search was conducted using Proteome Discoverer 2.4 and the Sequest HT search engine, with label-free quantitation. Each replicate was searched separately, and precursor ion area and abundances were not normalised as part of the label-free quantitation process.

Surface plasmon resonance studies

Kinetic analysis and equilibrium dissociation constants (K_D) were measured using a Biacore T200 system (Cytiva). The surfaces of flow cells one, two and four were activated for 14 min with a 1:1 mixture of 0.1 M NHS (*N*-hydroxysuccinimide) and 0.4 M EDC (*N*-(3-dimethylaminopropyl)-*N'*-ethylcarbodiimide hydrochloride) at a 5 μl/min flow rate. The ligands (AMA1) at a concentration of 80 μg/ml in 10 mM sodium acetate, pH 4.5, were immobilised at a density of 500 RU on flow cells two, three and four. Flow cell one was immobilised with bovine serum albumin to serve as a reference surface. All the surfaces were blocked with a 7-min injection of 1 M ethanolamine, pH 8.0. i-bodies (14 kDa, 90% purity based on SDS-PAGE) in 10 mM Tris, 150 mM NaCl,0.005% Tween-20,1% BSA pH 8, were injected over the flow cells at a concentration range at a flow rate of 45 μl/min and a temperature of 25 °C. Both multi-cycle kinetic and single-cycle kinetic analyses were used to describe the AMA1-i-body interactions.

Structure determination of the WD34-AMA1 complexes

WD34-bound *Pf*AMA1 and *Pv*AMA1 protein samples were prepared for crystallisation as described previously[29]. The protein-protein complexes were in 50 mM Tris (pH 8.0) and initial sparse matrix crystallisation trials were performed in 96-well sitting drop trays (Swissci, Neuheim, Switzerland) at a molar ratio of 1:1 using an in-house Gryphon LCP (Art Robbins Instruments). Initial screenings were set up with 0.2 μl protein sample and 0.2 μl reservoir per drop. Subsequent crystal optimisation trials were conducted in 24-well Limbro plates (Hampton Research). All crystallisation trials were performed at 20 °C. WD34-AMA1^{Pf} complex crystals were obtained in 0.1 M HEPES, 70% MPD, pH 7.5 at 5 mg/ml concentration and WD34-AMA1^{Pv} complex crystals were obtained in 0.1 M MES, 12% w/v PEG20000, pH 6.5 at 5 mg/ml concentration.

X-ray diffraction data was collected on the MXII beamline of Australian synchrotron using an Eiger detector (Dectris, Baden-Dättwil, Switzerland). Data were processed to 2.7 Å for WD34-AMA1^{Pf} and 3 Å for WD34-AMA1^{Pv} using the XDS package[73]. Structures were solved by molecular replacement in Phaser using the structural coordinates of PDB IDs—1Z40 (*Pf*AMA1), 5NQF (*Pv*AMA1) and 5AEA (i-body scaffold)[74,75]. Structure building and refinement were performed using Coot and PHENIX[76,77]. The atomic coordinates and structure files were deposited in the Protein Data Bank under PDB ID 8QU7 (WD34-AMA1^{Pf}) and 8QUS (WD34-AMA1^{Pv}). All the figures of the structures were prepared using PyMOL[78].

Blood-stage invasion inhibition assays

Two-cycle growth inhibition assays were performed as follows: synchronised trophozoite stage parasites were diluted to 0.5% parasitaemia (*P. knowlesi*) or 0.2% parasitaemia (*P. falciparum*) and 1% (v/v) haematocrit in 25 μl RPMI 1640, 25 mM HEPES media with i-bodies and added into 96-well round-bottomed culture plate. Parasites were incubated for 32 h (*P. knowlesi*) or 48 h (*P. falciparum*) at 37 °C. Parasites were then washed with PBS, stained with 10 μg/ml ethidium bromide (BioRad) and 1×10^5 erythrocytes were counted using an Accuri flow cytometer (BD Biosciences). i-body activity was assessed across three independent biological replicates and IC_{50} values were calculated using GraphPad Prism 9.2 (GraphPad, USA).

Blood-stage invasion inhibition assays for transgenic parasites

Invasion assays were performed with WD34 and 21H5 as previously described, with minor changes[79]. Parasites were synchronised with sorbitol, late trophozoite and schizont stages were then inoculated at 0.5% parasitaemia in 4% haematocrit in 45 μl RPMI media, with 5 μl i-bodies in PBS. The ring stages were harvested by fixing with 0.25%

glutaraldehyde. Parasites were stored in PBS at 4 °C. Cultures were later stained with 1× SYBR Green I (S7563, Invitrogen), and parasitaemia was assayed by flow cytometry in a BD FACSCanto™ II system, with further analysis in FlowJo™ v10.9.0 (BD Life Sciences). Parasites were gated from uninfected erythrocytes using the FITC-A and PE-A channels. Net growth rates were calculated by subtracting the parasitaemia of parasites inoculated with 1 mg/ml heparin, then dividing by the parasitaemia of parasites inoculated with 5 µl PBS. Growth percentages were subtracted from 100% to give invasion inhibition.

IC_{50} calculations were performed in R using the packages drc and ggplot2[79–82]. Assays were performed in biological triplicate, and IC_{50}s calculated independently for each replicate. The parasite lines used were based on W2mef, with the AMA1 locus replaced with either the *P. vivax* or the *P. falciparum* 3D7 locus[17,33].

Sporozoite cell traversal and hepatocyte invasion assays

HC-04 hepatocytes were seeded at near-confluence (100,000 cells per well) in 96-well plates[83]. *Plasmodium falciparum* NF54 sporozoites were generated by feeding stage V gametocytes at 0.3% parasitaemia to 3-day-old female *Anopheles stephensi* mosquitoes (kindly provided by M. Jacobs-Lorena, Johns Hopkins University) via water-jacketed glass membrane feeders as described[84]. On day 17 post bloodmeal, sporozoites were dissected from mosquito salivary glands in Scheider's medium, enumerated by a haemocytometer, and resuspended in IMDM + 5% FBS + 0.5 mg/ml FITC-dextran at a final concentration of 450 sporozoites/µl (multiplicity of infection [MOI]: 0.45). WD34 and 21H5 i-bodies were added at the indicated concentrations and incubated with sporozoites and FITC-dextran for 15 min on ice. mAb 2A10 against *P. falciparum* CSP (a kind gift from F. Zavala, Johns Hopkins University) was used as a positive control at 10 µg/ml to validate the assays. After incubation, sporozoites were added to cells and centrifuged at 500 × *g* for 3 min. After a 4 h incubation at 37 °C, 5% CO_2, cells were washed, trypsinised, and half of the cells processed to quantify cell traversal (percentage of FITC-Dextran positive HC-04 cells) by flow cytometry and the remaining half were replated in 96-well plates and incubated overnight at 37 °C, 5% CO_2 for quantification of invasion at 24 h post-infection (percentage of cells positive for anti-CSP conjugated to ALEXA 647) by flow cytometry, as previously described[85].

P. berghei infections in mice and Peters' 4-day suppressive test

Six to eight weeks old female BALB/c acceptor mice were injected intraperitoneally (I.P.) with 1×10^7 erythrocytes infected with *P. berghei* expressing mCherry-Luciferase (a kind gift from Volker Heussler) withdrawn from donor mice[86]. Mice were simultaneously treated with WD34 (30 mg/kg in a once-daily 'Q.D regimen', I.P.) for four consecutive days or chloroquine (50 mg/kg, I.P., once), or untreated control mice received PBS (vehicle). Twelve hours after administration of the last i-body dose, parasitaemias were measured by flow cytometry of mCherry-positive infected cells, as previously described[87]. Mean parasitaemia values in each group of 3–4 mice are expressed as percent parasitaemia. Giemsa-stained blood smears were used to confirm parasitaemia. All mice eventually developed patent infections and succumbed to malaria or were euthanised according to WEHI Animal Ethics Committee-approved procedures. Data were analysed by one-way ANOVA with multiple comparisons using GraphPad Prism 9.

Differential scanning fluorometry analysis

Melting temperatures and thermal stability of i-bodies were determined by the ViiA 7 real-time PCR system (ThermoFisher); 0.5 mg/ml and 1 mg/ml WD33 and WD34 i-bodies in PBS (pH 7.4) mixed with 10 × Sypro Orange Dye (Invitrogen). Samples were tested in duplicate starting at 25 °C and increasing in 0.5 °C steps, at a rate of 1 °C/min, to 95 °C. TAMRA reporter was set for excitation (~550 nm) and emission (~587 nm) channels. Data was normalised and a sigmoidal non-linear regression was performed using GraphPad Prism 9.2 (GraphPad, USA).

In vitro serum stability assay

WD34 was mixed with BALB/c mouse serum to a concentration of 100 µg/ml and incubated at 37 °C. Time-point samples (0, 6, 18, 24, 36, 48, 72 and 96 h) were collected and evaluated by ELISA for binding to AMA1 (Coating concentration, 1 µg/ml). mAb 5G8 was used as a reference for AMA1 binding.

Animal ethics statement

BALB/c mice were obtained from Jackson Laboratory and housed under Physical Containment level 2 conditions at La Trobe Animal Research and Training Facility (LARTF) and Walter and Elisa Hall Institute of Medical Research (WEHI) Animal Research facility. All procedures in the pharmacokinetic experiments were approved by the La Trobe University Animal Ethics Committee and performed in LARTF. All procedures in the *P. berghei* infection study were approved by the WEHI Animal Ethics Committee and performed at WEHI.

Pharmacokinetic study of WD34 by LC/MS-MS

Eight to ten weeks old male BALB/c mice ($n = 3$) were injected with a single dose of WD34 (30 mg/kg, I.P.) and blood samples were collected at 0.5, 6, 12, 24, and 48 h post-dosing. WD34 in the plasma was quantified by monitoring a signature peptide LTWSLGLPEATVNVK contained both CDR3 and framework residues of WD34, using liquid chromatography-tandem mass spectrometry, as described previously[55,88]. Briefly, serum samples were adjusted to 2% SDS in ammonium bicarbonate (20 mM), vortexed, and heated to 95 °C for 15 min, followed by sonication for 10 min. Lysate containing 40 µg of protein was reduced and alkylated with 5 mM tris (2-carboxyethyl) phosphine and 20 mM iodoacetamide. The single pot, solid phase, sample preparation strategy was used to clean up samples for mass spectrometry from solubilised lysates[89]. Proteins were captured onto carboxylate-modified magnetic SpeedBeads (Cytiva, Sweden), and beads were washed with 80% ethanol. Tryptic digestion was carried out in 20 mM ammonium bicarbonate overnight at 37 °C. The tryptic peptides were then desalted using the StageTip method and dried in a speedvac[72]. Tryptic peptides were separated on a Thermo Ultimate 3000 RSLCnano UHPLC system and analysed on a Thermo Q-Exactive HF Orbitrap mass-spectrometer (ThermoFisher Scientific, Waltham, MA, USA). Peptides (800 ng) were loaded onto an Acclaim PepMap C18 3 µm 0.075 mm × 20 mm trap column (ThermoFisher Scientific, Waltham, MA, USA) and washed at 5 µl/min for 6 min (Buffer C: 0.1% (v/v) trifluoracetic acid, 2% (v/v) ACN) before switching the pre-column in line with the analytical column held at 55 °C (nanoEase M/Z Peptide BEH C18 Column, 1.7 µm, 130 Å and 75 µm ID × 25 cm, Waters). The separation of peptides was performed at 250 nL/min using a linear Acetonitrile gradient. Blank runs were performed between sample injections.

Three injections per sample were performed in a 90-min run. CID MS/MS spectra were collected using a 90-min method with Orbitrap HCD parameters using Orbitrap HCD parameters. Dynamic exclusion parameters were set as follows: exclude isotope on, exclude after $n = 1$ times, duration 25 s, default charge state of 2, and use the peptide monoisotopic peak determination mode. Other instrument parameters were: MS1 scan at 60,000 resolution, m/z 350–1500, AGC target 3e6, injection time max 30 ms. The mass-spectral database search and quantitation were conducted using Skyline 23.1.0.380 and the MS Amanda search engine with label-free quantitation matched against the Mouse reference proteome (Downloaded March 2023) and the antibody sequence for WD34[90]. The peptide fixed mod was carbamidomethyl of C; no variable mods were set. Precursor charges set to 2, 3, and 0.05 m/z ion match tolerance. Precursor tolerance was set to 20 ppm and fragment tolerance to 0.05 Da. Digest was set to Trypsin, and

one missed cleavage was permitted. The included static modification was carbamidomethyl of C. Peptide quantification settings used MS1 precursor ion area and converted to ng protein using a matrix-matched calibration curve of WD34Fc in mouse serum (800 ng, 400 ng, 200 ng, 200 ng, 100 ng, 50 ng, 25 ng, 25 ng), with linear in log-space regression fit. WD34 abundance was normalised to mouse serum peptide MFASFPTTK (515.25733 m/z) to control technical variance.

Reporting summary

Further information on research design is available in the Nature Portfolio Reporting Summary linked to this article.

Data availability

The crystal structures reported in this manuscript are deposited in the Protein Data Bank, www.rcsb.org (PDB IDs 8QU7 and 8QUS). Source data are provided with this paper as a Source Data file.

References

1. World Health Organization. *World Malaria Report 2022* (WHO, 2022).
2. Phillips, M. A. et al. Malaria. *Nat. Rev. Dis. Prim.* **3**, 17050 (2017).
3. Phyo, A. P., Dahal, P., Mayxay, M. & Ashley, E. A. Clinical impact of vivax malaria: a collection review. *PLoS Med.* **19**, e1003890 (2022).
4. Miller, L. H., Ackerman, H. C., Su, X.-Z. & Wellems, T. E. Malaria biology and disease pathogenesis: insights for new treatments. *Nat. Med.* **19**, 156–167 (2013).
5. Gaur, D., Mayer, D. C. G. & Miller, L. H. Parasite ligand–host receptor interactions during invasion of erythrocytes by *Plasmodium* merozoites. *Int. J. Parasitol.* **34**, 1413–1429 (2004).
6. Baum, J., Maier, A. G., Good, R. T., Simpson, K. M. & Cowman, A. F. Invasion by *P. falciparum* merozoites suggests a hierarchy of molecular interactions. *PLoS Pathog.* **1**, e37 (2005).
7. Aikawa, M., Miller, L., Johnson, J. & Rabbege, J. Erythrocyte entry by malarial parasites. A moving junction between erythrocyte and parasite. *J. Cell Biol.* **77**, 72–82 (1978).
8. Barry, A. E. & Arnott, A. Strategies for designing and monitoring malaria vaccines targeting diverse antigens. *Front. Immunol.* **5**, 359 (2014).
9. Mitran, C. J. & Yanow, S. K. The case for exploiting cross-species epitopes in malaria vaccine design. *Front. Immunol.* **11**, 335 (2020).
10. Burns, A. L. et al. Targeting malaria parasite invasion of red blood cells as an antimalarial strategy. *FEMS Microbiol. Rev.* **43**, 223–238 (2019).
11. Besteiro, S., Michelin, A., Poncet, J., Dubremetz, J.-F. & Lebrun, M. Export of a *Toxoplasma gondii* rhoptry neck protein complex at the host cell membrane to form the moving junction during invasion. *PLoS Pathog.* **5**, e1000309 (2009).
12. Riglar, D. T. et al. Super-resolution dissection of coordinated events during malaria parasite invasion of the human erythrocyte. *Cell Host Microbe* **9**, 9–20 (2011).
13. Srinivasan, P. et al. Binding of *Plasmodium* merozoite proteins RON2 and AMA1 triggers commitment to invasion. *Proc. Natl Acad. Sci. USA* **108**, 13275–13280 (2011).
14. Yang, A. S. P. et al. AMA1 and MAEBL are important for *Plasmodium falciparum* sporozoite infection of the liver. *Cell. Microbiol.* **19**, e12745 (2017).
15. Fernandes, P. et al. The AMA1-RON complex drives *Plasmodium* sporozoite invasion in the mosquito and mammalian hosts. *PLoS Pathog.* **18**, e1010643 (2022).
16. Loubens, M. et al. *Plasmodium* sporozoites on the move: switching from cell traversal to productive invasion of hepatocytes. *Mol. Microbiol.* **115**, 870–881 (2021).
17. Drew, D. R. et al. Functional conservation of the AMA1 host-cell invasion ligand between *P. falciparum* and *P. vivax*: a novel platform to accelerate vaccine and drug development. *J. Infect. Dis.* **217**, 498–507 (2017).
18. Beeson, J. G. et al. Merozoite surface proteins in red blood cell invasion, immunity and vaccines against malaria. *FEMS Microbiol. Rev.* **40**, 343–372 (2016).
19. Kennedy, M. C. et al. In vitro studies with recombinant *Plasmodium falciparum* apical membrane antigen 1 (AMA1): production and activity of an AMA1 vaccine and generation of a multiallelic response. *Infect. Immun.* **70**, 6948–6960 (2002).
20. Bai, T. et al. Structure of AMA1 from *Plasmodium falciparum* reveals a clustering of polymorphisms that surround a conserved hydrophobic pocket. *Proc. Natl Acad. Sci. USA* **102**, 12736–12741 (2005).
21. Coley, A. M. et al. Structure of the malaria antigen AMA1 in complex with a growth-inhibitory antibody. *PLoS Pathog.* **3**, 1308–1319 (2007).
22. Hodder, A. N., Crewther, P. E. & Anders, R. F. Specificity of the protective antibody response to apical membrane antigen 1. *Infect. Immun.* **69**, 3286–3294 (2001).
23. Thera, M. A. et al. A field trial to assess a blood-stage malaria vaccine. *N. Engl. J. Med.* **365**, 1004–1013 (2011).
24. Remarque, E. J., Faber, B. W., Kocken, C. H. M. & Thomas, A. W. A diversity-covering approach to immunization with *Plasmodium falciparum* apical membrane antigen 1 induces broader allelic recognition and growth inhibition responses in rabbits. *Infect. Immun.* **76**, 2660–2670 (2008).
25. Dutta, S. et al. Overcoming antigenic diversity by enhancing the immunogenicity of conserved epitopes on the malaria vaccine candidate apical membrane antigen-1. *PLoS Pathog.* **9**, e1003840 (2013).
26. Kusi, K. A. et al. Safety and immunogenicity of multi-antigen AMA1-based vaccines formulated with CoVaccine HT™ and Montanide ISA 51 in rhesus macaques. *Malar. J.* **10**, 182 (2011).
27. Igonet, S. et al. Cross-reactivity studies of an anti-*Plasmodium vivax* apical membrane antigen 1 monoclonal antibody: binding and structural characterisation. *J. Mol. Biol.* **366**, 1523–1537 (2007).
28. Collins, C. R., Withers-Martinez, C., Hackett, F. & Blackman, M. J. An inhibitory antibody blocks interactions between components of the malarial invasion machinery. *PLoS Pathog.* **5**, e1000273 (2009).
29. Griffiths, K. et al. i-bodies, human single domain antibodies that antagonize chemokine receptor CXCR4. *J. Biol. Chem.* **291**, 12641–12657 (2016).
30. Streltsov, V. A. et al. Structural evidence for evolution of shark Ig new antigen receptor variable domain antibodies from a cell-surface receptor. *Proc. Natl Acad. Sci. USA* **101**, 12444–12449 (2004).
31. Cao, Q. et al. A single-domain i-body, AD-114, attenuates renal fibrosis through blockade of CXCR4. *JCI Insight* **7**, e143018 (2022).
32. Qiu, H. et al. ADR3, a next generation i-body to human RANKL, inhibits osteoclast formation and bone resorption. *J. Biol. Chem.* **299**, 102889 (2023).
33. Drew, D. R. et al. Defining the antigenic diversity of *Plasmodium falciparum* apical membrane antigen 1 and the requirements for a multi-allele vaccine against malaria. *PLoS ONE* **7**, e51023 (2012).
34. Terheggen, U. et al. Limited antigenic diversity of *Plasmodium falciparum* apical membrane antigen 1 supports the development of effective multi-allele vaccines. *BMC Med.* **12**, 183 (2014).
35. Coley, A. M. et al. The most polymorphic residue on *Plasmodium falciparum* apical membrane antigen 1 determines binding of an invasion-inhibitory antibody. *Infect. Immun.* **74**, 2628–2636 (2006).
36. Vulliez-Le Normand, B. et al. Structural and functional insights into the malaria parasite moving junction complex. *PLoS Pathog.* **8**, e1002755 (2012).
37. Elliott, S. R. et al. Research priorities for the development and implementation of serological tools for malaria surveillance. *F1000Prime Rep.* **6**, 100 (2014).
38. Lim, S. S. et al. Structure and dynamics of apical membrane antigen 1 from *Plasmodium falciparum* FVO. *Biochemistry* **53**, 7310–7320 (2014).

39. Vulliez-Le Normand, B., Saul, F. A., Hoos, S., Faber, B. W. & Bentley, G. A. Cross-reactivity between apical membrane antgen 1 and rhoptry neck protein 2 in *P. vivax* and *P. falciparum*: a structural and binding study. *PLoS ONE* **12**, e0183198 (2017).
40. Henderson, K. A. et al. Structure of an IgNAR-AMA1 complex: targeting a conserved hydrophobic cleft broadens malarial strain recognition. *Structure* **15**, 1452–1466 (2007).
41. Schymkowitz, J. et al. The FoldX web server: an online force field. *Nucleic Acids Res.* **33**, W382–W388 (2005).
42. Seidel-Greven, M. et al. Isolation and light chain shuffling of a *Plasmodium falciparum* AMA1-specific human monoclonal antibody with growth inhibitory activity. *Malar. J.* **20**, 37 (2021).
43. Maskus, D. J. et al. Characterization of a novel inhibitory human monoclonal antibody directed against *Plasmodium falciparum* apical membrane antigen 1. *Sci. Rep.* **6**, 39462 (2016).
44. Silvie, O. et al. A role for apical membrane antigen 1 during invasion of hepatocytes by *Plasmodium falciparum* sporozoites. *J. Biol. Chem.* **279**, 9490–9496 (2004).
45. Peters, W. The chemotherapy of rodent malaria, XXII. The value of drug-resistant strains of *P. berghei* in screening for blood schizontocidal activity. *Ann. Trop. Med. Parasitol.* **69**, 155–171 (1975).
46. Crewther, P. E., Matthew, M. L., Flegg, R. H. & Anders, R. F. Protective immune responses to apical membrane antigen 1 of *Plasmodium chabaudi* involve recognition of strain-specific epitopes. *Infect. Immun.* **64**, 3310–3317 (1996).
47. Dicko, A. et al. Impact of a *Plasmodium falciparum* AMA1 vaccine on antibody responses in adult Malians. *PLoS ONE* **2**, e1045 (2007).
48. Ouattara, A. et al. Lack of allele-specific efficacy of a bivalent AMA1 malaria vaccine. *Malar. J.* **9**, 175 (2010).
49. Henry, K. A. & MacKenzie, C. R. Antigen recognition by single-domain antibodies: structural latitudes and constraints. *mAbs* **10**, 815–826 (2018).
50. Drew, D. R. et al. Defining species-specific and conserved interactions of apical membrane protein 1 during erythrocyte invasion in malaria to inform multi-species vaccines. *Cell. Mol. Life Sci.* **80**, 74 (2023).
51. Scally, S. W. et al. PCRCR complex is essential for invasion of human erythrocytes by *Plasmodium falciparum*. *Nat. Microbiol.* **7**, 2039–2053 (2022).
52. Lyke, K. E. et al. Low-dose intravenous and subcutaneous CIS43LS monoclonal antibody for protection against malaria (VRC 612 Part C): a phase 1, adaptive trial. *Lancet Infect. Dis.* **23**, 578–588 (2023).
53. Lee, S.-K. et al. The direct binding of *Plasmodium vivax* AMA1 to erythrocytes defines a RON2-independent invasion pathway. *Proc. Natl Acad. Sci. USA* **120**, e2215003120 (2023).
54. Woehlbier, U., Epp, C., Hackett, F., Blackman, M. J. & Bujard, H. Antibodies against multiple merozoite surface antigens of the human malaria parasite *Plasmodium falciparum* inhibit parasite maturation and red blood cell invasion. *Malar. J.* **9**, 77 (2010).
55. Griffiths, K. et al. Half-life extension and non-human primate pharmacokinetic safety studies of i-body AD-114 targeting human CXCR4. *mAbs* **11**, 1331–1340 (2019).
56. Stanisic, D. I. & Good, M. F. Malaria vaccines: progress to date. *BioDrugs* **37**, 737–756 (2023).
57. Devi, S. 12 countries to get first doses of malaria vaccine. *Lancet* **402**, 172 (2023).
58. Datoo, M. S. et al. Efficacy and immunogenicity of R21/Matrix-M vaccine against clinical malaria after 2 years' follow-up in children in Burkina Faso: a phase 1/2b randomised controlled trial. *Lancet Infect. Dis.* **22**, 1728–1736 (2022).
59. Adepoju, P. RTS,S malaria vaccine pilots in three African countries. *Lancet* **393**, 1685 (2019).
60. Srinivasan, P. et al. Immunization with a functional protein complex required for erythrocyte invasion protects against lethal malaria. *Proc. Natl Acad. Sci. USA* **111**, 10311–10316 (2014).
61. Patel, P. N. et al. Structure-based design of a strain transcending AMA1-RON2L malaria vaccine. *Nat. Commun.* **14**, 5345 (2023).
62. Yanik, S. et al. Structure guided mimicry of an essential *P. falciparum* receptor-ligand complex enhances cross neutralizing antibodies. *Nat. Commun.* **14**, 5879 (2023).
63. Kisalu, N. K. et al. A human monoclonal antibody prevents malaria infection by targeting a new site of vulnerability on the parasite. *Nat. Med.* **24**, 408–416 (2018).
64. Kayentao, K. et al. Safety and efficacy of a monoclonal antibody against malaria in Mali. *N. Engl. J. Med.* **387**, 1833–1842 (2022).
65. Gaudinski, M. R. et al. A monoclonal antibody for malaria prevention. *N. Engl. J. Med.* **385**, 803–814 (2021).
66. Wu, R. L. et al. Low-dose subcutaneous or intravenous monoclonal antibody to prevent malaria. *N. Engl. J. Med.* **387**, 397–407 (2022).
67. Chandley, P., Ranjan, R., Kumar, S. & Rohatgi, S. Host-parasite interactions during *Plasmodium* infection: implications for immunotherapies. *Front. Immunol.* **13**, 1091961 (2023).
68. Trager, W. & Jensen, J. B. Continuous culture of *Plasmodium falciparum*: its impact on malaria research. *Int. J. Parasitol.* **27**, 989–1006 (1997).
69. Moon, R. W. et al. Adaptation of the genetically tractable malaria pathogen *Plasmodium knowlesi* to continuous culture in human erythrocytes. *Proc. Natl Acad. Sci. USA* **110**, 531–536 (2013).
70. Chatzileontiadou, D. S. M., Szeto, C., Jayasinghe, D. & Gras, S. Protein purification and crystallization of HLA-A∗02:01 in complex with SARS-CoV-2 peptides. *STAR Protoc.* **2**, 100635 (2021).
71. Minsky, A., Summers, R. G. & Knowles, J. R. Secretion of beta-lactamase into the periplasm of *Escherichia coli*: evidence for a distinct release step associated with a conformational change. *Proc. Natl Acad. Sci. USA* **83**, 4180–4184 (1986).
72. Rappsilber, J., Mann, M. & Ishihama, Y. Protocol for micro-purification, enrichment, pre-fractionation and storage of peptides for proteomics using StageTips. *Nat. Protoc.* **2**, 1896–1906 (2007).
73. Kabsch, W. XDS. *Acta Crystallogr. D Biol. Crystallogr.* **66**, 125–132 (2010).
74. McCoy, A. J. et al. Phaser crystallographic software. *J. Appl. Crystallogr.* **40**, 658–674 (2007).
75. McCoy, A. J., Grosse-Kunstleve, R. W., Storoni, L. C. & Read, R. J. Likelihood-enhanced fast translation functions. *Acta Crystallogr. D Biol. Crystallogr.* **61**, 458–464 (2005).
76. Emsley, P., Lohkamp, B., Scott, W. G. & Cowtan, K. Features and development of Coot. *Acta Crystallogr. D Biol. Crystallogr.* **66**, 486–501 (2010).
77. Adams, P. D. et al. PHENIX: a comprehensive Python-based system for macromolecular structure solution. *Acta Crystallogr. D Biol. Crystallogr.* **66**, 213–221 (2010).
78. The PyMOL Molecular Graphics System (Schrodinger LLC, 2015).
79. Persson, K. E. M., Lee, C. T., Marsh, K. & Beeson, J. G. Development and optimization of high-throughput methods to measure *Plasmodium falciparum*-specific growth inhibitory antibodies. *J. Clin. Microbiol.* **44**, 1665–1673 (2006).
80. Wickham, H. *ggplot2: Elegant Graphics for Data Analysis* (Springer, 2016).
81. R: A Language and Environment for Statistical Computing (R Foundation for Statistical Computing, 2023).
82. Ritz, C., Baty, F., Streibig, J. C. & Gerhard, D. Dose-response analysis using R. *PLoS ONE* **10**, e0146021 (2016).
83. Sattabongkot, J. et al. Establishment of a human hepatocyte line that supports in vitro development of the exo-erythrocytic stages of the malaria parasites *Plasmodium falciparum* and *P. vivax*. *Am. J. Trop. Med. Hyg.* **74**, 708–715 (2006).
84. Jennison, C. et al. Inhibition of plasmepsin V activity blocks *Plasmodium falciparum* gametocytogenesis and transmission to mosquitoes. *Cell Rep.* **29**, 3796–3806.e3794 (2019).

85. Lopaticki, S. et al. Tryptophan C-mannosylation is critical for *Plasmodium falciparum* transmission. *Nat. Commun.* **13**, 4400 (2022).
86. Prado, M. et al. Long-term live imaging reveals cytosolic immune responses of host hepatocytes against *Plasmodium* infection and parasite escape mechanisms. *Autophagy* **11**, 1561–1579 (2015).
87. Favuzza, P. et al. Dual plasmepsin-targeting antimalarial agents disrupt multiple stages of the malaria parasite life cycle. *Cell Host Microbe* **27**, 642–658.e612 (2020).
88. Marin, C. et al. Determination of plasma concentration of Belimumab by LC-MS/MS: method development, validation, and clinical application. *J. Pharm. Biomed. Anal.* **236**, 115730 (2023).
89. Hughes, C. S. et al. Single-pot, solid-phase-enhanced sample preparation for proteomics experiments. *Nat. Protoc.* **14**, 68–85 (2019).
90. Pino, L. K. et al. The Skyline ecosystem: informatics for quantitative mass spectrometry proteomics. *Mass Spectrom. Rev.* **39**, 229–244 (2020).

Acknowledgements

We thank Dr Kaye Truscott and Deepti Verghese Jose for facilitating the protein purification in MBB laboratory (La Trobe University), Dr Chris Szeto and Professor Stephanie Gras for training on SPR, Liana Theoridis and Dr Teresa Carvalho for supplying parasites for initial experiments, Ornella Romeo at Adelaide University for preparation of parasite samples, La Trobe Proteomics and Metabolomics Platform and Bioimaging Facility for facilitating SPR, confocal imaging and mass spectrometry services, AdAlta for providing reagents and consumables to conduct the study, Australian Red Cross Blood Service for blood. X-ray crystallographic data were acquired using the MX2 beamline at Australian Synchrotron, The Australian Nuclear Science and Technology Organization. D.A. was supported by La Trobe University Graduate Research Scholarship (LTGRS), and La Trobe University Full Fee Research Scholarship (LTUFFRS). J.C. and K.H.L. were supported by ARC-RTP Scholarships. D.W.W. acknowledges Hospital Research Foundation Fellowship and collaborative research grant. J.A.B. and J.G.B. acknowledge NHMRC Investigator Grants 1176955 and 1173046, respectively. The Burnet Institute is supported by NHMRC and Victorian State Government infrastructure grants.

Author contributions

M.F., R.F.A., and D.A. conceived the study. D.A., J.C., J.C.M., E.H., S.C., K.H.L., L.M.Y., J.M., D.H.O., C.C., and D.W.W. planned and performed the experiments. M.F., R.F.A., H.P., J.B., M.K., J.A.B., and D.W.W. supervised experiments. D.A., J.C., J.C.M., E.H., S.C., L.M.Y., J.A.B., and D.W.W. analysed the data. D.A., R.F.A., and M.F. wrote the original manuscript. All authors reviewed and approved the final manuscript.

Competing interests

This study was a collaboration between AdAlta Limited and La Trobe University. M.F. is the founding chief scientist and a shareholder in AdAlta Ltd., and R.F.A. is also a shareholder in AdAlta. The other authors have declared no competing interests.

Additional information

Supplementary information The online version contains supplementary material available at https://doi.org/10.1038/s41467-024-50770-7.

Correspondence and requests for materials should be addressed to Michael Foley.

Peer review information *Nature Communications* thanks Lea Barfod and the other anonymous reviewer(s) for their contribution to the peer review of this work. A peer review file is available.

Reprints and permissions information is available at http://www.nature.com/reprints

Publisher's note Springer Nature remains neutral with regard to jurisdictional claims in published maps and institutional affiliations.

[1]Department of Biochemistry and Chemistry, La Trobe Institute for Molecular Sciences, La Trobe University, Victoria 3086, Australia. [2]Research Centre for Infectious Diseases, School of Biological Sciences, The University of Adelaide, Adelaide, South Australia 5005, Australia. [3]Infectious Diseases & Immune Defense Division, The Walter and Eliza Hall Institute of Medical Research, 1G Royal Parade, Parkville, Victoria 3052, Australia. [4]Department of Medical Biology, The University of Melbourne, Parkville, Victoria 3052, Australia. [5]Burnet Institute, Melbourne, Victoria 3004, Australia. [6]Department of Medicine, The University of Melbourne, Parkville, Victoria 3052, Australia. [7]Central Clinical School and Department of Microbiology, Monash University, Clayton, Victoria 3800, Australia. [8]Department of Infectious Diseases, The University of Melbourne, Parkville, Victoria 3052, Australia. [9]Institute for Photonics and Advanced Sensing (IPAS), University of Adelaide, Adelaide, South Australia 5005, Australia. [10]AdAlta, Science Drive, Bundoora, Victoria 3083, Australia.
✉e-mail: m.foley@latrobe.edu.au